Indices of Pacific Walker Circulation strength: trends, correlations and uncertainty

Katarina Kosovelj[1], Žiga Zaplotnik[2], and Nedjeljka Žagar[3]

[1]University of Ljubljana
[2]European Centre for Medium-Range Weather Forecasts, Bonn, Germany
[3]Universität Hamburg, Meteorological Institute

January 3, 2023

Abstract

The strength of Pacific Walker circulation (PWC) significantly affects the global weather patterns, the distribution of mean precipitation, and modulates the rate of global warming. Different indices have been used to assess the PWC strength. Evaluated on different datasets for various study periods, the indices show large discrepancies between the reported trends. In this study, we performed sensitivity analysis of 10 PWC indices and compared them over the 1951-2020 period using the ERA5 reanalyses. The time series of normalised indices generally agree on the annual-mean PWC strength. The highest correlations (exceeding r=0.9) are between the indices that describe closely linked physical processes. The trends of PWC strength are strongly affected by the choice of representative time period. For the commonly used 1981-2010 period, the trends show strengthening of the PWC. However, trends computed for longer period (i.e. 1951-2020) are mostly neutral, whereas the past two decades (2000-2020) display weakening of the PWC, although it is statistically not significant. The temporal evolution of trends suggests multidecadal variability of PWC strength with a period of about 35 years, implying a continued weakening of the PWC in the next decade.

Indices of Pacific Walker Circulation strength: trends, correlations and uncertainty

K. Kosovelj[1], Ž. Zaplotnik[1,2], N. Žagar[3]

[1]Faculty of Mathematics and Physics, University of Ljubljana, Ljubljana, 1000, Slovenia
[2]European Centre for Medium-Range Weather Forecasts, Bonn, Germany
[3]Meteorological Institute, Center for Earth System Research and Sustainability, Universität Hamburg, 20146 Hamburg, Germany

Key Points:

- The evolution and trends of the Pacific Walker circulation (PWC) are evaluated using ten PWC indices in ERA5 data in the 1951-2020 period.
- Trends are strongly affected by the choice of representative time period and are rarely statistically significant.
- Positive and negative trends are suggestive of the presence of a multidecadal oscillation in the PWC.

Corresponding author: Katarina Kosovelj, `katarina.kosovelj@fmf.uni-lj.si`

Abstract

The strength of Pacific Walker circulation (PWC) significantly affects the global weather patterns, the distribution of mean precipitation, and modulates the rate of global warming. Different indices have been used to assess the PWC strength. Evaluated on different datasets for various study periods, the indices show large discrepancies between the reported trends. In this study, we performed sensitivity analysis of 10 PWC indices and compared them over the 1951-2020 period using the ERA5 reanalyses.

The time series of normalised indices generally agree on the annual-mean PWC strength. The highest correlations (exceeding $r = 0.9$) are between the indices that describe closely linked physical processes.

The trends of PWC strength are strongly affected by the choice of representative time period. For the commonly used 1981-2010 period, the trends show strengthening of the PWC. However, trends computed for longer period (i.e. 1951-2020) are mostly neutral, whereas the past two decades (2000-2020) display weakening of the PWC, although it is statistically not significant. The temporal evolution of trends suggests multidecadal variability of PWC strength with a period of about 35 years, implying a continued weakening of the PWC in the next decade.

Plain Language Summary

The Pacific Walker circulation (PWC) is tropical atmospheric circulation that consists of easterly winds close to the ground, westerlies aloft, upward motion in the western and downward motion over the eastern Pacific. The PWC impacts the rate of global warming and the sea-level rise. Thus, its accurate representation and prediction is an ultimate goal of climate models.

Towards this goal, the PWC strength has been described by a number of indices. Evaluated on different datasets and for various study periods, the PWC indices show large discrepancies between the reported trends. We assessed (dis)agreement among 10 PWC indices for 1951-2020 period using the ERA5 dataset, as the most reliable representation of the climate system since 1950. The indices computed from ERA5 data verify well with observations.

Indices generally agree on time series of PWC strength, with the highest correlations between the indices based on closely linked physical processes. However, we show

that the PWC trends are strongly affected by the choice of representative time period and often not statistically significant. They overall suggest weakening of PWC in the last two decades. Moreover, oscillatory structure of the trends suggest the presence of multidecadal oscillation of PWC.

1 Introduction

The Pacific Walker circulation (PWC) is the zonal part of the overturning tropical Pacific circulation, driven by the zonal pressure gradient and associated with the longitudinal gradients of sea-surface temperature. The PWC is characterized by the ascending motion over the warmer western Pacific east of around 150°E, and descending motion over the cooler eastern Pacific west of around 90°W (Peixoto & Oort, 1992; Seager et al., 2019). The circulation cell is completed by the upper-tropospheric equatorial westerlies and lower-tropospheric equatorial easterlies. The magnitude of the involved horizontal and vertical motions defines the PWC strength.

The strength of PWC is largely synced with the Pacific ocean circulation via the Bjerknes feedback (Bjerknes, 1969). Thus, it crucially impacts the global climate; it affects the precipitation distribution in the tropics (e.g., Barichivich et al., 2018) as well as in extratropics via atmospheric teleconnections, it is coupled to the mean-sea level in the tropical Pacific (e.g., Merrifield, 2011; Muis et al., 2018), impacts heat uptake (e.g., Meehl et al., 2011; England et al., 2014; McGregor et al., 2014), carbon uptake and carbon outgassing (Betts et al., 2020) and therefore also the rate of climate-change-induced warming in tropics and extratropics, particularly in winter when the heat-transporting stationary/transient eddies are stronger (Kosaka & Xie, 2013). Therefore, a comprehensive description and accurate prediction of PWC is of great societal importance.

Several distinct metrics have been used in the literature to date to describe the PWC strength and its changes in time. These metrics have been applied to distinct observational and reanalysis datasets for distinct time periods. For example, Sohn and Park (2010) related the PWC strength to the magnitude of the water vapor transport in the lower return branch of PWC. Using satellite data (from microwave imager and infrared sounder) and reanalyses, they reported a PWC strengthening in the 1979-2007 period. Similar conclusions were reached by Sohn et al. (2013) for the 1979-2008 period using purely observational datasets and different metrics including sea-surface-temperature (SST) and sea-level-pressure (SLP) differences across the equatorial Pacific. Kociuba and Power (2015) applied an identical SLP index and observed significant strengthening in the 1980-2012 period, whereas any trend starting before 1951 and ending in 2012 is negative. Strengthening of the PWC in recent decades was suggested also by Chen et al. (2008); Luo et al. (2012); Meng et al. (2012); L'Heureux et al. (2013); Bayr et al. (2014); Sandeep et al. (2014); Chung et al. (2019); Zhao and Allen (2019), as well as by the isotopic analysis of δ^{18}O (Falster et al., 2021). The PWC strengthening in turn lead to increased zonal sea-surface temperature (SST) gradients in the equatorial Pacific (Seager et al., 2019), and enhanced upwelling of the cold deep-ocean water in the Eastern Pacific, causing the so-called global warming hiatus in the 2000s and early 2010s (Kosaka & Xie, 2013; England et al., 2014; Watanabe et al., 2013).

In contrast, a number of studies reported a weakening trend of PWC, in particular for indices evaluated using numerical modeling. Bellomo and Clement (2015) related the vertical velocity in the PWC's ascending branch to the observed cloud cover and argued for a weakening PWC trend for the 1954-2008 period, consistent with the projected weakening by the climate models due to anthropogenic climate change (Knutson & Manabe, 1995; Held & Soden, 2006; Vecchi et al., 2006; Vecchi & Soden, 2007; Bayr et al., 2014; Wu et al., 2021; Masson-Delmotte et al., 2021). PWC weakening between 1950 and 2009 has been also suggested by Tokinaga et al. (2012) who analyzed the SLP gradient over the tropical Pacific derived from the atmospheric general circulation model (AGCM) experiments forced by the SSTs from the International Comprehensive Ocean–Atmosphere Data Set (ICOADS, Woodruff et al., 2011), instead of the more commonly used HadISST1 data (Rayner et al., 2003). Other studies reporting a weakening trend of the Walker circulation in the 20th century include Deser et al. (2010), Power and Kociuba (2011) and DiNezio et al. (2013). This was supported by the isotopic analysis of corals in the tropical Pacific (Liu et al., 2019).

The examples above reveal opposite conclusions about the trends of PWC strength using different datasets and metrics of PWC strength. The PWC time series reflect a combination of forced signal and multidecadal climate variability, making a direct intercomparison of various studies difficult, even for largely-overlapping periods. While a strengthening of the PWC in the period after 1979 seems firmly established (Wu et al., 2021), its near-future projection is less clear. It is necessary to systematically intercompare the PWC indices in use and their sensitivity to the analysis periods for the computation of the trends. We carry out such a comparison in this paper. The paper complements previous studies by L'Heureux et al. (2013), Plesca et al. (2018) and Chung et al. (2019) that compared the PWC trends for several PWC indices, by performing a systematic intercomparison of ten PWC indices used in the literature up to date on the latest generation of the European reanalyses, ERA5.

We evaluate the ten indices using the ECMWF ERA5 dataset in the 1951-2020 period (Hersbach et al., 2020), we test their sensitivity to averaging regions and levels, and verify them with their equivalents derived directly from observations. The definitions of 10 indices and details about various datasets are provided in Section 2. The time series of PWC indices, their correlations, and the sensitivity of the derived trends to different periods are compared in Section 3. Conclusions and discussions are given in Section 4.

2 Pacific Walker Circulation Indices and Datasets

We present ten indices, that are considered suitable given results from their recent applications and understanding of tropical east-west circulation.

2.1 Definitions of Indices

The following indices of Pacific Walker Circulation are compared:

1. Point-based Southern oscillation index (SOI) from Troup (1965), which is defined by the anomaly in the mean sea-level pressure difference between Tahiti and Darwin station data standardized for each month of the year using 1950-2021 as a base period. As we compute the SOI from the reanalysis data, the closest model gridpoints are used for evaluation (see Supplementary Information Fig. S1 for justification).

2. Area-averaged Southern oscillation index ΔSLP from Vecchi et al. (2006), defined as a difference between anomalies in mean sea-level pressure over the eastern and western equatorial Pacific. The anomalies are averaged over two boxes, both extending from 5°S to 5°N in meridional directions. In zonal direction the boxes extend from 80°E to 160°E (western Pacific box) and from 80°W to 160°W (eastern Pacific box). This index has been widely used due to the availability of long-term historical data on sea-level pressure.

3. Velocity potential index from Tanaka et al. (2004) that is computed for 2D circulation at a single vertical level (typically pressure p level) by solving the Poisson equation

$$\nabla \cdot \mathbf{V}_p = -\nabla^2 \chi_p. \tag{1}$$

The index was originally defined by Tanaka et al. (2004) as the yearly average of maximum deviation of velocity potential from its zonal mean over equatorial Pacific at 200 hPa level, χ_{200}. Here, the yearly averaging was applied as a 12-month running mean. However, as the maximum divergent outflow from a convective area over the Maritime continent is higher up in the troposphere (see Fig. S2) and varies year-to-year, we rather constructed a data-adaptive index $\chi_{\max}$, which takes the maximal velocity potential over equatorial Pacific at each time step (see Section 3 for argumentation and Fig. S3 for justification).

4. Vertical velocity index from Wang (2002) (named ω_{500}), calculated as the difference in average vertical pressure velocity anomalies between eastern and western equatorial Pacific at 500 hPa. Eastern Pacific is defined as an area between 120°W and 160°W, and from 5°S to 5°N). The Western Pacific is defined between 120°E and 160°E, and from 5°S to 5°N).

5. The sea-surface temperature (SST) index defined the same way as the ΔSLP index, but for the SST data. SST data are often used as a proxy/driver for PWC strength (Tokinaga et al., 2012; Meng et al., 2012; Zhang & Karnauskas, 2017).

6. Effective wind for water vapor transport index following Sohn and Park (2010). The boundary layer easterlies in the lower return branch of the Walker circulation carry the water vapor from the eastern to the western Pacific to provide additional fuel for condensation heating, which maintains the Walker circulation. The increase and decrease of water vapor flux, normalized by the total amount of vapor in the atmospheric column, is regarded as the strengthening and weakening of circulation, respectively. The effective wind is defined as:

$$\mathbf{V}_e = \sum_{i=1}^{N} \frac{PW\,(i)}{TPW}\,\mathbf{V}_D\,(i)\,, \tag{2}$$

where PW(i) is precipitable water in a vertical layer between i-th and $i+1$-th vertical level, TPW is the total precipitable water in a column and $\mathbf{V}_D(i)$ is divergent wind at i-th vertical level. The summation goes from the ground level upwards (in our case from 1000 hPa to 850 hPa).

Precipitable water $PW(i)$ is calculated as

$$PW(i) = \frac{1}{\rho_w g} \int_{p_i}^{p_{i+1}} q(p)\,\mathrm{d}p, \tag{3}$$

where ρ_w is water density, g is gravity acceleration, $q(p)$ is specific humidity, and p_i and p_{i+1} are boundaries of specific layer ($p_{i+1} < p_i$). Total precipitable water is calculated in the same way, with $p_i = p_s$ (surface pressure) and p_{i+1} is at the top of the atmosphere.

As we are interested in Walker circulation, we only used the zonal component of the divergent wind (u_D) and defined the index (named V_e) as an average value of effective zonal wind for water vapor transport in the tropical Pacific area (120°E to 120°W, and 5°S to 5°N).

7. Stream function index, based on a mass stream function:

$$\psi(p) = \frac{2\pi a}{g} \int_0^p u\,\mathrm{d}p, \tag{4}$$

where a is the radius of the Earth, g is gravity acceleration, and u is the zonal component of wind averaged between 5°S and 5°N. We define the index (named ψ_{500}) as maximal stream function at 500 hPa within 90°E and 80°W. Originally this index was defined using the zonal component of divergent wind (Yu & Zwiers, 2010; Bayr et al., 2014). Whereas the divergent circulation explains the majority of the meridional tropical circulation (Pikovnik et al., 2022), the zonal response to deep convective forcing over the Maritime continent projects on both the rotational and divergent flows (Gill, 1980). Thus, we opted for the zonal component of the total wind instead of its divergent part (their difference is shown in Fig. S4).

8. Zonally-integrated (across the Pacific basin) wind stress following Clarke and Lebedev (1996), i.e. L_τ. It is defined as

$$L_\tau = \int_0^L \overline{\tau_x}\,\mathrm{d}x, \tag{5}$$

where $\overline{\tau_x}$ is meridionally averaged zonal wind stress. Zonal integration is performed between 124°E and 90°W. In the meridional direction, we choose to average between 5°S and 5°N, to be consistent with other indices. Following Clarke and Lebedev (1996), we computed wind stress as

$$\tau_x = \rho_a c_D \left|\mathbf{V}\right| u, \tag{6}$$

where ρ_a is air density (with a constant value of 1.2 kg/m^3 as in Clarke and Lebedev (1996)), c_D is drag coefficient (1.5×10^{-3}), and $\mathbf{V}$ is horizontal surface wind vector at 10 m elevation ($\mathbf{V} = (u, v)$).

9. Upper tropospheric specific humidity (denoted Q_{200}). As the upper-tropospheric water vapor in the western equatorial Pacific is mainly transported by deep convection in the ascending branch of the PWC, a change in the upper-tropospheric humidity may indicate a change in the circulation strength (Sohn et al., 2013). To eliminate the increase of specific humidity (a general increase in humidity due to global atmospheric warming), we formulated the index as the difference in upper tropospheric humidity at the top of ascending and descending branches of Walker circulation. The humidity Walker circulation index is then defined as a difference in average specific humidity between two boxes over the eastern and western Pacific at 200 hPa. We used the same horizontal boxes for specific humidity as they were used for ω_{500}.

10. Average surface zonal winds over the central equatorial Pacific (denoted U_{ave}), after Chung et al. (2019). The index is applied by averaging 10 m wind over an area from 6°S to 6°N and from 180° to 150°W.

The ten indices can be grouped into two categories: (a) the direct circulation indices (χ_{max}, ψ_{500}, L_τ, U_{ave}, $\mathbf{V}_e$ and ω_{500}) which directly measure the velocity of the flow or associated flow function in any of the PWC branches, and (b) the indirect indices of the PWC magnitude derived from the atmospheric mass field or the lower boundary (Q_{200}, SOI, ΔSLP and SST). The Q_{200} index measures PWC strength through the convective humidity-influx in the upper troposphere, whereas the SST index measures the PWC strength through coupled ocean-atmosphere interactions.

All indices are influenced also by other parts of the tropical general circulation, i.e. by the Hadley and Monsoon circulations. In particular, indices that indirectly measure PWC strength and may not only be representative of the PWC changes but also of the accompanying local Hadley cells (Sohn et al., 2019; Pikovnik et al., 2022; Zaplotnik et al., 2022). The anthropogenic warming of the atmosphere and increasing water content directly affect the thermodynamic indices, whereas the SST index is also affected by the ocean processes.

Some of the indices attain physical units, some are made dimensionless, and they may have largely different magnitude. To make indices comparable, we standardize them, i.e. the mean value of the index is subtracted from each index and then normalized by its standard deviation within the study period. All indices are computed for 1950-2021 period. As application of running mean shortens time series of χ indices for six month at each end of the interval, the comparison of indices is performed on 1951-2020 period.

The indices require different amounts of data for their evaluation. SOI is calculated from pressure in two particular locations and can be affected by the local microclimate, especially when computed from station measurements, whereas indices from area-averaged data (ΔSLP, ω_{500}, SST, $\mathbf{V}_e$, L_τ, Q_{200}, U_{ave}) should better represent large processes. Some of the indices require only one basic variable and are easily calculated (e.g. SOI, ΔSLP, SST, Q_{200}, U_{ave}), while others require derived products (e.g. ψ_{500}, $\chi_{\max}$, L_τ, $\mathbf{V}_e$) and/or more complex calculation (e.g. ψ_{500}, $\mathbf{V}_e$). It is therefore logical that historically, the choice of the PWC index was influenced by the availability of data and computational resources.

2.2 Data

To intercompare a range of PWC indices, a dataset based on fully-coupled atmosphere-ocean modeling is required. The latest ERA5 reanalysis data are used for the period 1950-2021 (Hersbach et al., 2020, 2018a; Bell et al., 2020a). The indices are derived from the pressure vertical velocity ω, the zonal and meridional winds and specific humidity, which are provided on a regular latitude-longitude grid with 1° horizontal resolution and 27 vertical pressure levels, extending from 100 to 1000 hPa. Sea surface temperature (SST) data and the mean-sea-level pressure (MSLP) data are at the same horizontal grid (Hersbach et al., 2018b; Bell et al., 2020b). Depending on the index, we use either monthly means, computed from either daily 00 UTC data for horizontal winds (u and v) or daily means for all other variables (MSLP, ω, specific humidity q, and sea-surface temperature SST). The mixed-use of 00 UTC and daily mean data was justified by comparison of both datasets for the ωindex at 500 hPa, as the ω is one of the variables most affected by the diurnal cycle. However, the choice of 00 UTC or daily mean data has negligible impact on the indices (see Fig. S5).

We consider ERA5 sufficient for the analysis for several reasons. First, Simmons (2022) has shown that ERA5 very well verifies with the upper-tropospheric wind measurements in the tropics. The mean departure between the observations and background or first-guess in data assimilation (i.e. short-range forecasts) for upper-tropospheric zonal winds is trend-free and less than 1 m/s from the late 1990s onwards. In addition, the supplemental material includes our verification of PWC indices based on surface winds in ERA5 and the Wave- and Anemometer-based Sea surface wind product (WASWind, Tokinaga & Xie, 2011) showing their close correspondence (Fig. S6). Similarly, the ERA5-derived SST indices agree well with the indices derived from HadISST data (Rayner et al. (2003); see Fig. S7 for comparison). The same applies to the SOI index based on ERA5 data verified against the index derived from raw station data (Fig. S1).

3 Results

In this section we first discuss temporal evolution of the ten indices (including their reformulations in two cases) and correlation coefficients between various indices. This is followed by the evaluation of trends and their sensitivity to the period used for the computation of the trends.

3.1 Time-series of PWC indices and their correlations

Time series of the normalised annual-mean PWC indices (Fig. 1a) agree relatively well on the evolution and relative strength of PWC during most of the period since 1950. The majority of the indices spot strong El Niños in e.g. 1972, 1982/83, 1987, 1992, 1997/98, and 2015. There is more discrepancy between the indices regarding La Niñas, as they tend to be more prolonged. The two indices that deviate most from the others are the stream function index based on the divergent zonal wind at 500 hPa and velocity potential at 200 hPa. Their more poor agreement with other indices motivated their reformulation as described in the previous section and discussed below.

The fact that different indices describe different aspects of PWC implies that their correlations will vary (Fig. 1b). Correlations are generally high between the indices derived from physically linked processes. For example, the pair of indices with the high-

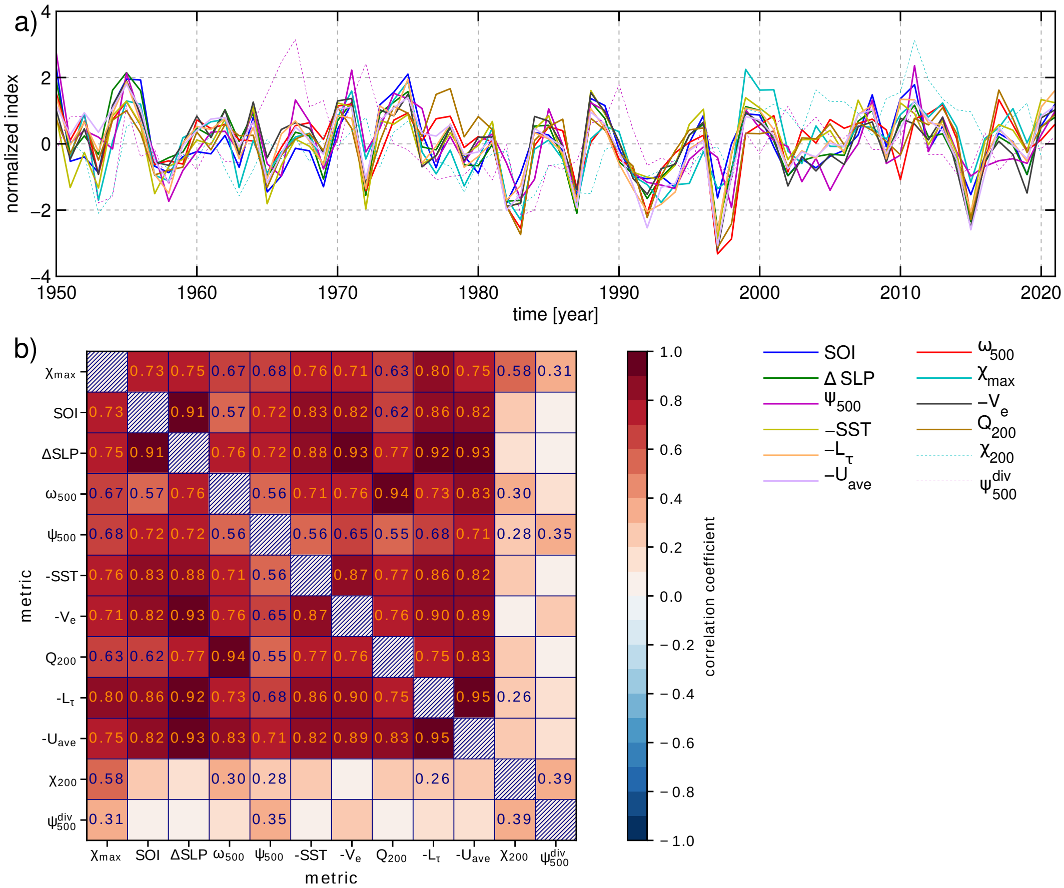

Figure 1. a) Time series of annual-mean PWC strength in ERA5 reanalysis between 1950 and 2021 for different PWC indices described in Section 2.1 as shown in the legend. b) Correlations between annual means of different PWC indices. Statistically significant (at 95 % confidence level) correlation coefficients are written in the respective fields. SST, V_e, L_τ and U_{ave} indices are multiplied by (-1) for easier comparison with other indices. χ_{200} and $\psi_{500}^{\mathrm{div}}$ are shown dashed in a) as they are replaced by better defined equivalent indices and not used in the continuation.

est correlation coefficient ($r = 0.95$) is U_{ave} and L_τ, which both describe surface easterlies. The ω index very highly correlates ($r = 0.94$) with the Q-index, as the amount of upper tropospheric humidity is directly related to the magnitude of vertical water vapor transport through convection. Similarly, the ΔSLP index correlates very highly ($r =$ 0.92 to 0.93) with the zonal surface wind index U_{ave}, surface wind stress index L_τ, and zonal boundary-layer moisture transport (represented by the effective wind V_e). This can be expected, as the pressure difference (expressed by SOI, ΔSLP) over the Pacific drives the near-surface equatorial easterlies. The larger the pressure difference, the stronger the easterlies (U_{ave}), the wind stress (L_τ), and the water vapor transport (V_e).

The correlations are somewhat lower between indices derived from distinct processes, e.g. surface wind and upper-tropospheric humidity ($r = 0.83$). Moderate correlations are observed between ω, and SST and ΔSLP indices with $r = 0.71$ and 0.76, respectively. This suggests, that the convective mass flux over the Maritime continent is controlled not only by the zonal SST gradient or SLP gradient but also by the local meridional gradients in the Western Pacific (Sohn et al., 2019). This is further supported by a rather moderate correlation ($r = 0.56$) between the SST and ψ indices, suggested also by He et al. (2014).

The original χ_{200} index (Tanaka et al., 2004) and stream-function index ψ_{500}^{div} (Yu & Zwiers, 2010; Bayr et al., 2014) (both indicated with dashed line in Fig. 1a) stand out from the rest and do not properly distinguish between the strongest El Niños. After the year 2000, χ_{200}-index also significantly exceeds the values of other indices. The velocity-potential index is highly susceptible to the choice of upper-tropospheric pressure level, in connection to the strong vertical profile of the divergent outflow (see Figs. S2, S3). The peak divergent outflow also occurs at different pressure levels year-to-year. Therefore an index defined at some predetermined pressure level can miss peak velocity potential. To alleviate it, we constructed a data-adaptive index, which takes the maximum of monthly-mean χ at any level within the box area. Such index correlates almost perfectly with the χ_{150} index ($r = 0.98$), meaning that the original χ_{200} index was applied too low in the troposphere. Our reformulated index χ_{max} verifies much better with other PWC indices (Fig. 1b).

Similarly, the stream-function index computed from total zonal wind instead of the zonal divergent wind verifies well with other PWC indices. The original stream-function index based on the divergent wind deviates from other indices in particular in the pre-satellite era in the 1960s and 1970s (see Figs. 1a and S8). Correlations with other indices are small, and the only statistically significant correlations for annual means are with χ_{200}, $\chi_{\max}$ and ψ_{500} indices (r between 0.3 and 0.4).

PWC indices are typically defined at fixed vertical levels where the underlying physical processes are on average the strongest; for example, the divergent outflow is strongest in the upper troposphere at around 150 hPa level (Fig. S2) and the stream function has largest amplitude at 500 hPa level. As the PWC strength and position oscillate on a year-to-year basis, the intercomparison of PWC indices might be skewed due to the displacement of maxima from vertical levels on which indices are computed. To ensure that our results are not significantly affected by such displacements, we tested the sensitivity of the indices to meaningful changes in the choice of the vertical level. The sensitivity was checked for χ, ω, ψ, and Q indices (see Figs. S3, S5, S8, and S9). We also checked the sensitivity of indices to different meridional extents of horizontal areas used in their computation (see Fig. S8 for ψ and Fig. S9 for Q-index). As the tropical processes are mainly centered at the ITCZ, we checked how the indices, originally defined in a narrow equatorial belt (5°S and 5°N) change when meridional borders of the areas considered were modified (5°N and 20°N) to better align with the average position of ITCZ. This was applied to V_e, ψ, L_τ, and Q indices. In general, the indices are not very sensitive to the vertical level or horizontal area used for calculation, as long as the chosen level/area is close to the level/area used in the original definition. This is supported by high correlation coefficients between different variations of each index (not shown). The only exception is the χ index, which varies significantly with the vertical level used for computation, as already mentioned. Our sensitivity analysis confirms that the results on PWC changes, presented in this paper, are not meaningfully impacted by the mild shifts of vertical levels or meridional averaging.

3.2 Trends in PWC and their sensitivity to the WC

The PWC trends are evaluated from time series of standardized annual-mean PWC indices using linear regression. Figure 2 shows trends computed starting from various years from 1951 to 2000, with the end year of the interval fixed to 2020. This figure shows that the trends depend on the starting year. Most indices show neutral-to-negative trends for the start year between 1951 and 1970, suggesting that PWC has remained steady or has been slightly weakening in the recent 70-year or 50-year time period. The exceptions to this rule are the velocity-potential index and the SST index, which show strengthening of PWC until nearly the end of 20th century. In the 1980-2020 period, the PWC has been strengthening according to most of the PWC indices. However, only $\chi_{\max}$, ω_{500} and L_τ indices show statistically significant strengthening at the 95% confidence level according to the modified, trend free, pre-whitening Mann-Kendall test (Yue & Wang, 2002; Hussain & Mahmud, 2019) (see Table S1). This applies also to the 1990-2020 period with one half of the indices showing statistically significant trends. In the recent two decades (2000-2020 period), the majority of the indices suggests PWC weakening, although the uncertainty is relatively large.

Next question to ask is how the trends vary if both the end and start year for the computation of the trend vary. This is shown in Fig. 3. Three distinct areas can be identified in the figure, although not equally clear for all ten indices: 1) trends, starting in the 1950s, and ending in the 1970s are mostly positive, suggesting an increase in PWC strength; 2) trends, starting approximately between 1960 and 1980, and ending around 2010 are mostly negative and often statistically significant, suggesting a weakening of PWC; 3) trends, starting between around 1980 and mid to late 1990s are again mostly positive, regardless of the end year. On the other hand, long-term trends starting before the mid-1970s and ending after the year 2010 are insignificant and have even different signs.

The right diagonal line shows 20-year running trends with start years from 1951 to 2000. This suggests approximately 20 years of downtrend (blue colours, start years 1963 to 1980) followed by 20 years of uptrend (red colours, start years 1980 to 1997). Together, this suggests a multidecadal variability of the PWC with an approximately 35-year period. If so, blue patches in the upper-right corners of Fig. 3, that indicate a PWC weakening, together with recent trends in Fig. 2 suggest that a multidecadal trend reversal might be just taking place. Although a further analysis with longer dataset is needed to confirm that the trends are associated with a multidecadal oscillation in PWC, our expectation of a weakened PWC in the coming years agree with Wu et al. (2021) who reached their conclusion by coupling the PWC with the Interdecadal Pacific Oscillation.

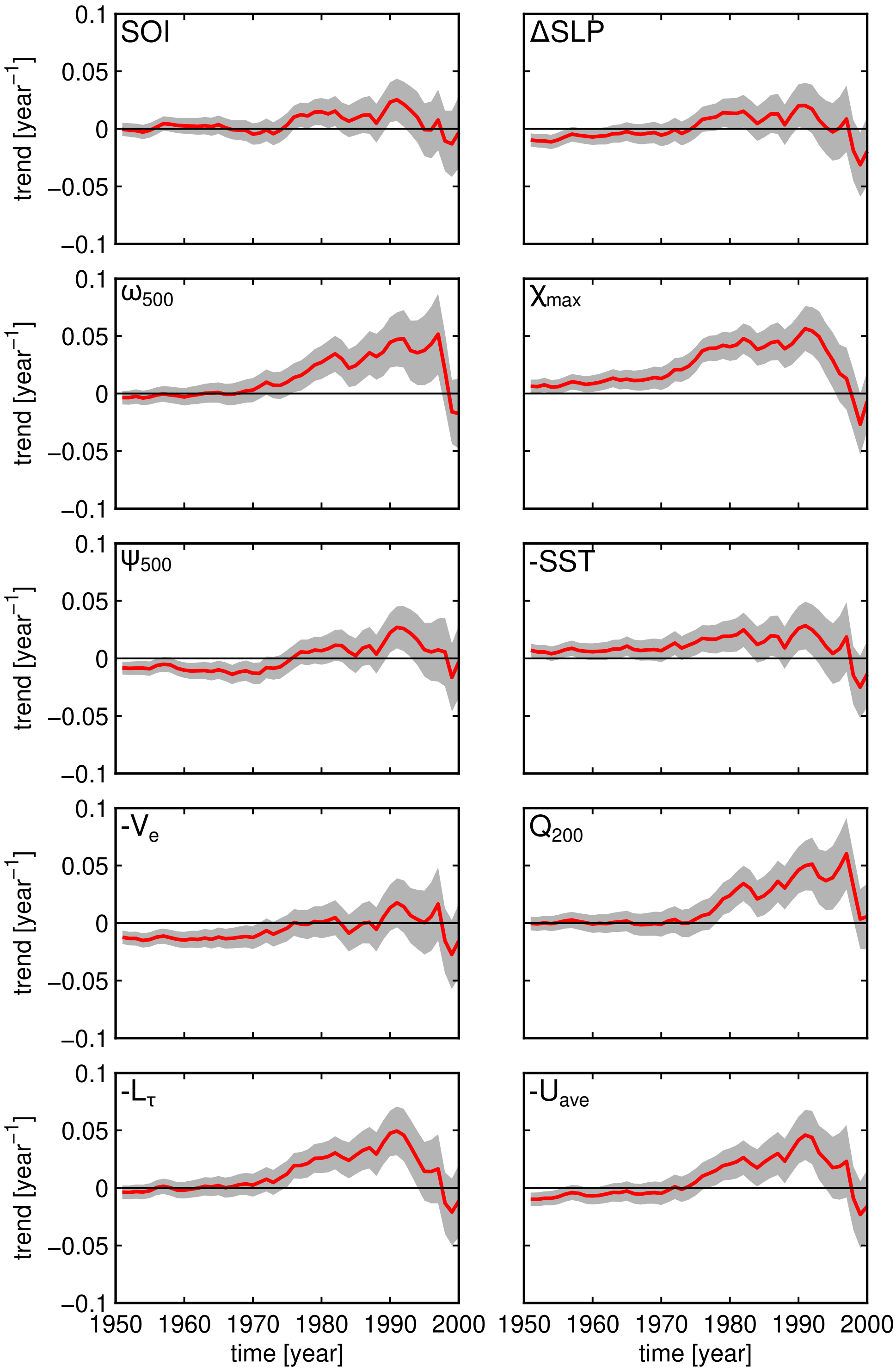

Figure 2. Trends of Pacific Walker circulation (PWC) strength as a function of the starting year of the trend for different PWC indices. The end year of all linear trends is fixed to 2020. For example, the year 1970 on the x-axis represents the PWC trend calculated for 1970-2020. PWC trends for periods shorter than 20 years are not shown. Thick red lines represent the trend value, and the gray areas represent the uncertainty (i.e. plus or minus one standard deviation) of the estimated trend. SST, V_e, L_τ and U_{ave} indices are multiplied by (-1) for easier comparison with other indices.

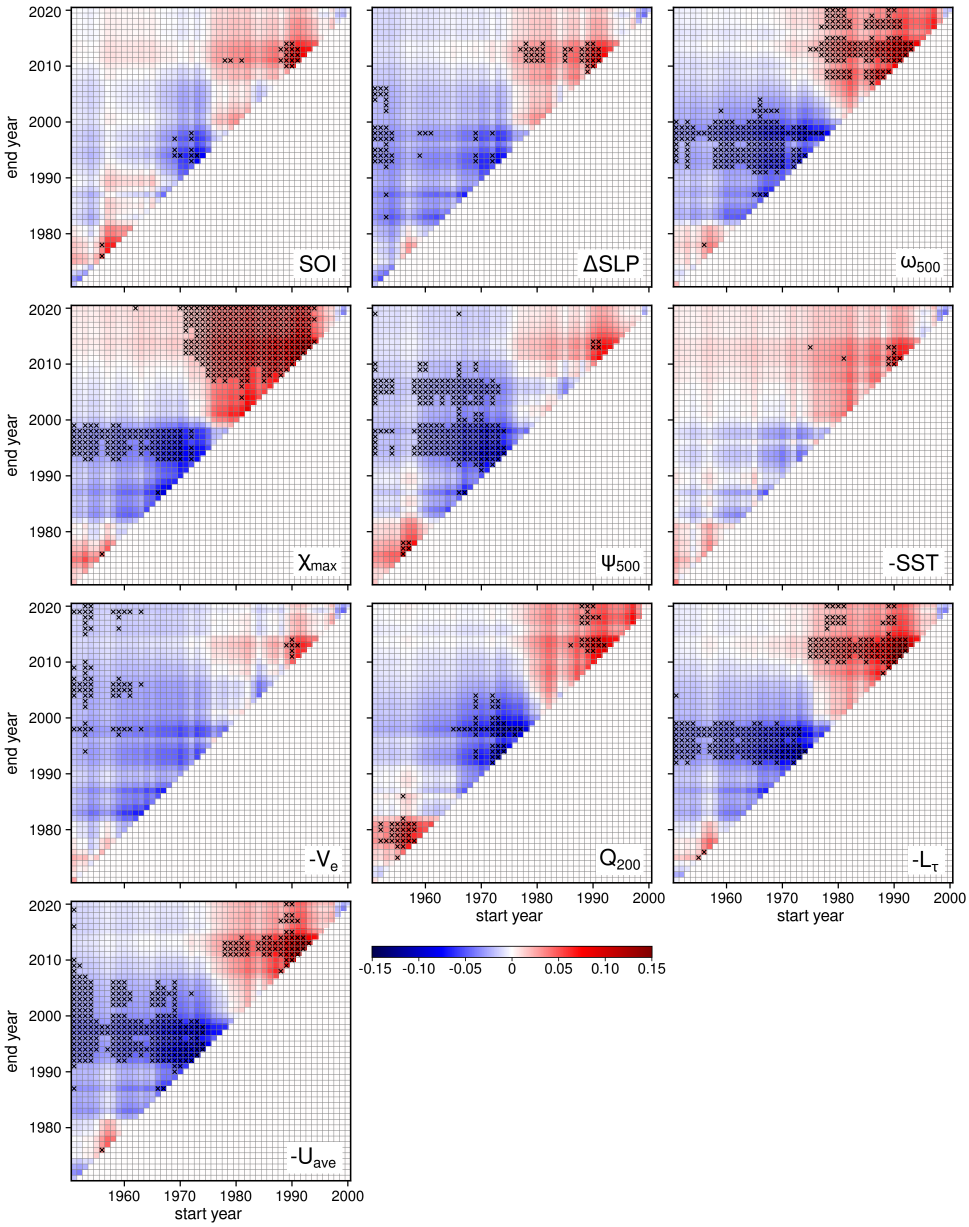

Figure 3. Trends of Pacific Walker circulation (PWC) strength as a function of the starting year (x-axis) and end year (y-axis) of the trend for different PWC indices. PWC trends for periods shorter than 20 years are not shown. Crosses represent statistically significant trends at the 95% confidence level. SST, V_e L_τ and U_{ave} indices are multiplied by (-1) for easier comparison with other indices. The checkered pattern is a result of ENSO variability. First row in the matrix is a realisation of Fig. 2. The bottom-left top-right diagonal (0-diagonal) effectively represents a 20-year running trend (as in e.g. L'Heureux et al., 2013), whereas the k-diagonal represents a $(20 + k)$-year running trend.

4 Discussion and Conclusions

The study compares ten different indices of the Pacific Walker circulation (PWC) strength over the 1951-2020 period using the ECMWF ERA5 reanalyses. We have shown that the indices derived from ERA5 are equivalent to indices deduced from the raw observation data, as ERA5 accurately verifies with the observations of upper-tropospheric zonal winds, zonal surface winds, sea-level pressure, sea-surface temperature (see Supplementary information and Hersbach et al., 2020; Simmons, 2022). Some PWC indices have been refined. For example, the χ index was originally defined at 200 hPa (Tanaka et al., 2004). However, the newest state-of-the-art datasets suggest that the maximum divergent outflow associated with convection over the western Pacific is higher in the troposphere, at around 150 hPa. Similarly, the original definition of the stream function index is based on divergent wind (Yu & Zwiers, 2010; Bayr et al., 2014) and appears to miss an important part of the zonal tropical circulation associated with the PWC. Thus, we suggest to replace χ_{200} and ψ_{500} by χ_{max} and $\psi_{500}^{\mathrm{tot}}$, respectively.

In general, the normalized PWC indices agree regarding the variation of annual-mean PWC strength (see Fig. 1a). The correlations are highest ($r = 0.9$ or more) between the indices which describe closely linked processes, as could be expected. The indices are most often based on a single level. We have shown that the sensitivity of indices to the reasonable changes in the choice of vertical level or horizontal averaging area is negligible. One exception is the velocity potential index, which displays strong sensitivity to the choice of vertical level.

The sensitivity of the trends to the applied periods is often poorly explored in the literature. Our study shows that different indices, different lengths of the applied interval, and their start and end years, can largely affect the trends and their significance. In the common climatological reference period 1981-2010, the majority of indices showed PWC strengthening. On the longer time scales, i.e. 1951-2020, the trend is mostly neutral and insignificant. Furthermore, the majority of indices suggest that the PWC might have been weakening during the last two decades (2000-2020). A continuation of this trend implies a reversal of the PWC into an El Niño-type state with decreased ocean heat uptake and more rapid global warming. We suggest that the observed variability in the trends of the PWC indices is associated with the multidecadal variability of the PWC with a period of about 35 years. Longer data series are needed to confirm this result.

The recent (1981-2010) PWC strengthening has been unequivocally opposed to the climate model projections (Gulev et al., 2021). Whether the source of the discrepancy is multidecadal variability as seen in Fig. 3 (Meng et al., 2012; Chung et al., 2019; Wu et al., 2021), forced response (Mann et al., 2021; Orihuela-Pinto et al., 2022) or biases in the coupled ocean-atmosphere climate models (Durack et al., 2012; McGregor et al., 2014; Seager et al., 2019; Watanabe et al., 2020; Wills et al., 2022), caution should be exercised for the detection and comparison of PWC trends in the models and reanalyses. We speculate a shift toward weakening of the PWC. If realised, it will crucially impact the global distribution of precipitation in the tropics and extratropics, the ocean heat uptake (e.g. Meehl et al., 2011), the sea-level rise and the rate of global warming.

Appendix A Open Research

ERA5 data (https://doi.org/10.24381/cds.bd0915c6, Hersbach et al., 2018) was downloaded from the Copernicus Climate Change Service (C3S) Climate Data Store (last access 27 June 2022). The results contain modified Copernicus Climate Change Service information 2022. Neither the European Commission nor ECMWF is responsible for any use that may be made of the Copernicus information or data it contains.

Scripts for calculation of indices and data used to generate Figs. 1-3 and S1-S12 are published in Zenodo data repository: https://doi.org/10.5281/zenodo.7359879 (Kosovelj et al., 2022).

Acknowledgments

This research has been supported by the Javna Agencija za Raziskovalno Dejavnost RS (grant no. J1-9431 and Programme P1-0188). Research of Nedjeljka Žagar contributes to Germany's Excellence Strategy—EXC 2037 'CLICCS—Climate, Climatic Change, and Society'-project number: 390683824, contribution to the Center for Earth System Research and Sustainability (CEN) of Universität Hamburg.

The Authors thank Matic Pikovnik (Slovenian Environment Agency, ARSO, and University of Ljubljana, Faculty of Mathematics and Physics) for sharing parts of the code that contributed to this research.

References

Barichivich, J., Gloor, E., Peylin, P., Brienen, R. J., Schöngart, J., Espinoza, J. C., & Pattnayak, K. C. (2018). Recent intensification of Amazon flooding extremes driven by strengthened Walker circulation. *Science Advances*, *4*(9). Retrieved from `https://www.science.org/doi/10.1126/sciadv.aat8785` doi: 10.1126/SCIADV.AAT8785/SUPPL{_}FILE/AAT8785{_}SM.PDF

Bayr, T., Dommenget, D., Martin, T., & Power, S. B. (2014). The eastward shift of the Walker Circulation in response to global warming and its relationship to ENSO variability. *Climate Dynamics*, *43*(9-10), 2747–2763. doi: 10.1007/s00382-014-2091-y

Bell, B., Hersbach, H., Berrisford, P., Dahlgren, P., Horányi, A., Muñoz Sabater, J., ... Thépaut, J.-N. (2020a). *ERA5 hourly data on pressure levels from 1950 to 1978 (preliminary version).* Copernicus Climate Change Service (C3S) Climate Data Store (CDS). Retrieved from `https://cds.climate.copernicus-climate.eu/cdsapp#!/dataset/reanalysis-era5-pressure-levels-preliminary-back-extension?tab=overview`

Bell, B., Hersbach, H., Berrisford, P., Dahlgren, P., Horányi, A., Muñoz Sabater, J., ... Thépaut, J.-N. (2020b). *ERA5 hourly data on single levels from 1950 to 1978 (preliminary version).* Copernicus Climate Change Service (C3S) Climate Data Store (CDS). Retrieved from `https://cds.climate.copernicus-climate.eu/cdsapp#!/dataset/reanalysis-era5-single-levels-preliminary-back-extension?tab=overview`

Bellomo, K., & Clement, A. C. (2015, 9). Evidence for weakening of the Walker circulation from cloud observations. *Geophysical Research Letters*, *42*(18), 7758–7766. Retrieved from `https://onlinelibrary.wiley.com/doi/full/10.1002/2015GL065463https://onlinelibrary.wiley.com/doi/abs/10.1002/2015GL065463` doi: 10.1002/2015GL065463

Betts, R. A., Burton, C. A., Feely, R. A., Collins, M., Jones, C. D., & Wiltshire, A. J. (2020). ENSO and the Carbon Cycle. *Geophysical Monograph Series*, *253*, 453–470. Retrieved from `https://onlinelibrary.wiley.com/doi/full/10.1002/9781119548164.ch20https://onlinelibrary.wiley.com/doi/abs/10.1002/9781119548164.ch20https://agupubs.onlinelibrary.wiley.com/doi/10.1002/9781119548164.ch20` doi: 10.1002/9781119548164.CH20

Bjerknes, J. (1969). Atmospheric Teleconnetions from the Equatorial Pacific. *Monthly Weather Review*, *97*(3), 163–172. Retrieved from `https://journals.ametsoc.org/view/journals/mwre/97/3/1520-0493_1969_097_0163_atftep_2_3_co_2.xml` doi: 10.1175/1520-0493(1969)097⟨0163:ATFTEP⟩2.3.CO;2

Chen, J., Del Genio, A. D., Carlson, B. E., & Bosilovich, M. G. (2008). The Spatiotemporal Structure of Twentieth-Century Climate Variations in Observations and Reanalyses. Part I: Long-Term Trend. *Journal of Climate*, *21*(11), 2611–2633. Retrieved from `https://journals.ametsoc.org/view/journals/clim/21/11/2007jcli2011.1.xml` doi: 10.1175/2007JCLI2011.1

Chung, E. S., Timmermann, A., Soden, B. J., Ha, K. J., Shi, L., & John, V. O. (2019). Reconciling opposing Walker circulation trends in observations and model projections. *Nature Climate Change*, *9*(5), 405–412. Retrieved from `https://doi.org/10.1038/s41558-019-0446-4` doi: 10.1038/s41558-019-0446-4

Clarke, A. J., & Lebedev, A. (1996). Long-Term Changes in the Equatorial Pacific Trade Winds. *Journal of Climate*, *9*(5), 1020–1029.

Deser, C., Phillips, A. S., & Alexander, M. A. (2010). Twentieth century tropical sea surface temperature trends revisited. *Geophysical Research Letters*, *37*(10). Retrieved from `https://onlinelibrary.wiley.com/doi/full/10.1029/2010GL043321` doi: 10.1029/2010GL043321

DiNezio, P. N., Vecchi, G. A., & Clement, A. C. (2013). Detectability of Changes in the Walker Circulation in Response to Global Warming. *Journal of Climate*, *26*(12), 4038–4048. Retrieved from `https://journals.ametsoc.org/view/journals/clim/26/12/jcli-d-12-00531.1.xml` doi: 10.1175/JCLI-D-12-00531.1

Durack, P. J., Wijffels, S. E., & Matear, R. J. (2012). Ocean salinities reveal strong global water cycle intensification during 1950 to 2000. *Science*, *336*(6080), 455–458. Retrieved from `https://www.science.org/doi/10.1126/science.1212222` doi: 10.1126/SCIENCE.1212222/SUPPL{_}FILE/DURACK.SM.PDF

England, M. H., Mcgregor, S., Spence, P., Meehl, G. A., Timmermann, A., Cai, W., … Santoso, A. (2014). Recent intensification of wind-driven circulation in the Pacific and the ongoing warming hiatus. *Nature Climate Change*, *4*(3), 222–227. doi: 10.1038/nclimate2106

Falster, G., Konecky, B., Madhavan, M., Stevenson, S., & Coats, S. (2021). Imprint of the Pacific Walker Circulation in Global Precipitation δ18O. *Journal of Climate*, *34*(21), 8579–8597. Retrieved from https://journals.ametsoc.org/view/journals/clim/34/21/JCLI-D-21-0190.1.xml doi: 10.1175/JCLI-D-21-0190.1

Gill, A. E. (1980). Some simple solutions for heat-induced tropical circulation. *Quarterly Journal of the Royal Meteorological Society*, *106*(449), 447–462. doi: 10.1002/qj.49710644905

Gulev, S. K., Thorne, P. W., Ahn, J., Dentener, F. J., Domingues, C. M., Gerland, S., ... Vose, R. S. (2021). Changing State of the Climate System. In V. Masson-Delmotte et al. (Eds.), *Climate change 2021: The physical science basis. contribution of working group i to the sixth assessment report of the intergovernmental panel on climate change* (chap. 2). Cambridge, United Kingdom and New York, NY, USA: Cambridge University Press. Retrieved from https://www.ipcc.ch/report/ar6/wg1/downloads/report/IPCC_AR6_WGI_Chapter_02.pdf

He, J., Soden, B. J., & Kirtman, B. (2014). The robustness of the atmospheric circulation and precipitation response to future anthropogenic surface warming. *Geophysical Research Letters*, *41*(7), 2614–2622. Retrieved from https://onlinelibrary.wiley.com/doi/full/10.1002/2014GL059435https://onlinelibrary.wiley.com/doi/abs/10.1002/2014GL059435https://agupubs.onlinelibrary.wiley.com/doi/10.1002/2014GL059435 doi: 10.1002/2014GL059435

Held, I. M., & Soden, B. J. (2006). Robust responses of the hydrological cycle to global warming. *Journal of Climate*, *19*(21), 5686–5699. Retrieved from http://journals.ametsoc.org/jcli/article-pdf/19/21/5686/3800493/jcli3990_1.pdf doi: 10.1175/JCLI3990.1

Hersbach, H., Bell, B., Berrisford, P., Biavati, G., Horányi, A., Muñoz Sabater, J., ... Thépaut, J.-N. (2018a). *ERA5 hourly data on pressure levels from 1959 to present.* Copernicus Climate Change Service (C3S) Climate Data Store (CDS). Retrieved from https://doi.org/10.24381/cds.bd0915c6 doi: 10.24381/cds.bd0915c6

Hersbach, H., Bell, B., Berrisford, P., Biavati, G., Horányi, A., Muñoz Sabater, J., ... Thépaut, J.-N. (2018b). *ERA5 hourly data on single levels from 1959 to present.* Copernicus Climate Change Service (C3S) Climate Data Store (CDS). Retrieved from `https://doi.org/10.24381/cds.adbb2d47` doi: 10.24381/cds.adbb2d47

Hersbach, H., Bell, B., Berrisford, P., Hirahara, S., Horányi, A., Muñoz-Sabater, J., ... Thépaut, J. N. (2020). The ERA5 Global Reanalysis. *Quarterly Journal of the Royal Meteorological Society*, *146*(730), 1999–2049. Retrieved from `https://rmets.onlinelibrary.wiley.com/doi/full/10.1002/qj.3803` doi: 10.1002/qj.3803

Hussain, M. M., & Mahmud, I. (2019). pyMannKendall: a python package for non parametric Mann Kendall family of trend tests. *Journal of Open Source Software*. Retrieved from `https://doi.org/10.21105/joss.01556` doi: 10.21105/joss.01556

Knutson, T. R., & Manabe, S. (1995). Time-mean response over the tropical Pacific to increased CO2 in a coupled ocean-atmosphere model. *Journal of Climate*, *8*(9), 2181–2199. Retrieved from `https://journals.ametsoc.org/view/journals/clim/8/9/1520-0442_1995_008_2181_tmrott_2_0_co_2.xml` doi: 10.1175/1520-0442(1995)008⟨2181:TMROTT⟩2.0.CO;2

Kociuba, G., & Power, S. B. (2015). Inability of CMIP5 Models to Simulate Recent Strengthening of the Walker Circulation: Implications for Projections. *Journal of Climate*, *28*(1), 20–35. Retrieved from `https://journals.ametsoc.org/view/journals/clim/28/1/jcli-d-13-00752.1.xml` doi: 10.1175/JCLI-D-13-00752.1

Kosaka, Y., & Xie, S. P. (2013). Recent global-warming hiatus tied to equatorial Pacific surface cooling. *Nature*, *501*(7467), 403–407. Retrieved from `http://dx.doi.org/10.1038/nature12534` doi: 10.1038/nature12534

Kosovelj, K., Zaplotnik, Z., & Zagar, N. (2022). *Indices of Pacific Walker Circulation strength: trends, correlations and uncertainty (submitted version).* doi: https://doi.org/10.5281/zenodo.7359879

L'Heureux, M. L., Lee, S., & Lyon, B. (2013, 3). Recent multidecadal strengthening of the Walker circulation across the tropical Pacific. *Nature Climate Change 2013 3:6*, *3*(6), 571–576. Retrieved from `https://www.nature.com/articles/`

nclimate1840 doi: 10.1038/nclimate1840

Liu, Z., Jian, Z., Poulsen, C. J., & Zhao, L. (2019, 2). Isotopic evidence for twentieth-century weakening of the Pacific Walker circulation. *Earth and Planetary Science Letters*, *507*, 85–93. doi: 10.1016/J.EPSL.2018.12.002

Luo, J. J., Sasaki, W., & Masumoto, Y. (2012, 11). Indian Ocean warming modulates Pacific climate change. *Proceedings of the National Academy of Sciences of the United States of America*, *109*(46), 18701–18706. Retrieved from https://www.pnas.org/doi/abs/10.1073/pnas.1210239109 doi: 10.1073/PNAS.1210239109/SUPPL{_}FILE/PNAS.201210239SI.PDF

Mann, M. E., Steinman, B. A., Brouillette, D. J., & Miller, S. K. (2021, 3). Multidecadal climate oscillations during the past millennium driven by volcanic forcing. *Science*, *371*(6533), 1014–1019. Retrieved from https://science.sciencemag.org/content/371/6533/1014https://science.sciencemag.org/content/371/6533/1014.abstract doi: 10.1126/SCIENCE.ABC5810

Masson-Delmotte, V., et al. (Eds.). (2021). *IPCC, 2021: Climate Change 2021: The Physical Science Basis. Contribution of Working Group I to the Sixth Assessment Report of the Intergovernmental Panel on Climate Change.*

McGregor, S., Timmermann, A., Stuecker, M. F., England, M. H., Merrifield, M., Jin, F. F., & Chikamoto, Y. (2014). Recent walker circulation strengthening and pacific cooling amplified by atlantic warming. *Nature Climate Change*, *4*(10), 888–892. doi: 10.1038/nclimate2330

Meehl, G. A., Arblaster, J. M., Fasullo, J. T., Hu, A., & Trenberth, K. E. (2011, 9). Model-based evidence of deep-ocean heat uptake during surface-temperature hiatus periods. *Nature Climate Change 2011 1:7*, *1*(7), 360–364. Retrieved from https://www.nature.com/articles/nclimate1229 doi: 10.1038/nclimate1229

Meng, Q., Latif, M., Park, W., Keenlyside, N. S., Semenov, V. A., & Martin, T. (2012). Twentieth century Walker Circulation change: Data analysis and model experiments. *Climate Dynamics*, *38*(9-10), 1757–1773. Retrieved from https://link.springer.com/article/10.1007/s00382-011-1047-8 doi: 10.1007/S00382-011-1047-8/FIGURES/13

Merrifield, M. A. (2011, 8). A Shift in Western Tropical Pacific Sea Level

Trends during the 1990s. *Journal of Climate*, *24*(15), 4126–4138. Retrieved from https://journals.ametsoc.org/view/journals/clim/24/15/2011jcli3932.1.xml doi: 10.1175/2011JCLI3932.1

Muis, S., Haigh, I. D., Guimarães Nobre, G., Aerts, J. C., & Ward, P. J. (2018, 9). Influence of El Niño-Southern Oscillation on Global Coastal Flooding. *Earth's Future*, *6*(9), 1311–1322. Retrieved from https://onlinelibrary.wiley.com/doi/full/10.1029/2018EF000909https://onlinelibrary.wiley.com/doi/abs/10.1029/2018EF000909https://agupubs.onlinelibrary.wiley.com/doi/10.1029/2018EF000909 doi: 10.1029/2018EF000909

Orihuela-Pinto, B., England, M. H., & Taschetto, A. S. (2022, 6). Interbasin and interhemispheric impacts of a collapsed Atlantic Overturning Circulation. *Nature Climate Change 2022 12:6*, *12*(6), 558–565. Retrieved from https://www.nature.com/articles/s41558-022-01380-y doi: 10.1038/s41558-022-01380-y

Peixoto, J. P., & Oort, A. H. (1992). *Physics of climate.* American Institute of Physics.

Pikovnik, M., Zaplotnik, Z., Boljka, L., & Žagar, N. (2022, 6). Metrics of the Hadley circulation strength and associated circulation trends. *Weather and Climate Dynamics*, *3*(2), 625–644. doi: 10.5194/WCD-3-625-2022

Plesca, E., Grützun, V., & Buehler, S. A. (2018, 1). How Robust Is the Weakening of the Pacific Walker Circulation in CMIP5 Idealized Transient Climate Simulations? *Journal of Climate*, *31*(1), 81–97. Retrieved from https://journals.ametsoc.org/view/journals/clim/31/1/jcli-d-17-0151.1.xml doi: 10.1175/JCLI-D-17-0151.1

Power, S. B., & Kociuba, G. (2011). What Caused the Observed Twentieth-Century Weakening of the Walker Circulation? *Journal of Climate*, *24*(24), 6501–6514. Retrieved from https://journals.ametsoc.org/view/journals/clim/24/24/2011jcli4101.1.xml doi: 10.1175/2011JCLI4101.1

Rayner, N. A., Parker, D. E., Horton, E. B., Folland, C. K., Alexander, L. V., Rowell, D. P., … Kaplan, A. (2003, 7). Global analyses of sea surface temperature, sea ice, and night marine air temperature since the late nineteenth century. *Journal of Geophysical Research: Atmospheres*, *108*(D14), 4407. Retrieved from https://onlinelibrary.wiley.com/doi/full/10.1029/

2002JD002670https://onlinelibrary.wiley.com/doi/abs/10.1029/2002JD002670https://agupubs.onlinelibrary.wiley.com/doi/10.1029/2002JD002670 doi: 10.1029/2002JD002670

Sandeep, S., Stordal, F., Sardeshmukh, P. D., & Compo, G. P. (2014, 4). Pacific Walker Circulation variability in coupled and uncoupled climate models. *Climate Dynamics*, *43*(1-2), 103–117. Retrieved from https://link.springer.com/article/10.1007/s00382-014-2135-3 doi: 10.1007/S00382-014-2135-3/FIGURES/9

Seager, R., Cane, M., Henderson, N., Lee, D. E., Abernathey, R., & Zhang, H. (2019, 7). *Strengthening tropical Pacific zonal sea surface temperature gradient consistent with rising greenhouse gases* (Vol. 9) (No. 7). Nature Publishing Group. Retrieved from https://doi.org/10.1038/s41558-019-0505-x doi: 10.1038/s41558-019-0505-x

Simmons, A. J. (2022, 7). Trends in the tropospheric general circulation from 1979 to 2022. *Weather and Climate Dynamics*, *3*(3), 777–809. doi: 10.5194/WCD-3-777-2022

Sohn, B. J., & Park, S.-C. (2010, 8). Strengthened tropical circulations in past three decades inferred from water vapor transport. *Journal of Geophysical Research*, *115*(D15), D15112. Retrieved from http://doi.wiley.com/10.1029/2009JD013713 doi: 10.1029/2009JD013713

Sohn, B. J., Yeh, S. W., Lee, A., & Lau, W. K. (2019, 3). Regulation of atmospheric circulation controlling the tropical Pacific precipitation change in response to CO2 increases. *Nature Communications*, *10*(1), 1–8. Retrieved from https://www.nature.com/articles/s41467-019-08913-8 doi: 10.1038/s41467-019-08913-8

Sohn, B. J., Yeh, S. W., Schmetz, J., & Song, H. J. (2013, 4). Observational evidences of Walker circulation change over the last 30 years contrasting with GCM results. *Climate Dynamics*, *40*(7-8), 1721–1732. Retrieved from https://link.springer.com/article/10.1007/s00382-012-1484-z doi: 10.1007/S00382-012-1484-Z/FIGURES/5

Tanaka, H. L., Ishizaki, N., & Kitoh, A. (2004, 5). Trend and interannual variability of Walker, monsoon and Hadley circulations defined by velocity potential in the upper troposphere. *Tellus A*, *56*(3), 250–269. Retrieved from http://tellusa.net/index.php/tellusa/article/view/14410 doi: 10.1111/j.1600-0870.2004.00049.x

Tokinaga, H., & Xie, S. P. (2011, 1). Wave- and Anemometer-Based Sea Surface Wind (WASWind) for Climate Change Analysis. *Journal of Climate*, *24*(1), 267–285. Retrieved from https://journals.ametsoc.org/view/journals/clim/24/1/2010jcli3789.1.xml doi: 10.1175/2010JCLI3789.1

Tokinaga, H., Xie, S. P., Deser, C., Kosaka, Y., & Okumura, Y. M. (2012, 11). Slowdown of the Walker circulation driven by tropical Indo-Pacific warming. *Nature 2012 491:7424*, *491*(7424), 439–443. Retrieved from https://www.nature.com/articles/nature11576 doi: 10.1038/nature11576

Troup, A. J. (1965, 10). The 'southern oscillation'. *Quarterly Journal of the Royal Meteorological Society*, *91*(390), 490–506. Retrieved from https://onlinelibrary.wiley.com/doi/full/10.1002/qj.49709139009https://onlinelibrary.wiley.com/doi/abs/10.1002/qj.49709139009https://rmets.onlinelibrary.wiley.com/doi/10.1002/qj.49709139009 doi: 10.1002/QJ.49709139009

Vecchi, G. A., & Soden, B. J. (2007, 9). Global Warming and the Weakening of the Tropical Circulation. *Journal of Climate*, *20*(17), 4316–4340. Retrieved from http://journals.ametsoc.org/doi/10.1175/JCLI4258.1 doi: 10.1175/JCLI4258.1

Vecchi, G. A., Soden, B. J., Wittenberg, A. T., Held, I. M., Leetmaa, A., & Harrison, M. J. (2006, 5). Weakening of tropical Pacific atmospheric circulation due to anthropogenic forcing. *Nature 2006 441:7089*, *441*(7089), 73–76. Retrieved from https://www.nature.com/articles/nature04744 doi: 10.1038/nature04744

Wang, C. (2002, 2). Atmospheric circulation cells associated with the El Nino-Southern Oscillation. *Journal of Climate*, *15*(4), 399–419. Retrieved from https://journals.ametsoc.org/view/journals/clim/15/4/1520-0442_2002_015_0399_accawt_2.0.co_2.xml doi: 10.1175/1520-0442(2002)015⟨0399:ACCAWT⟩2.0.CO;2

Watanabe, M., Dufresne, J. L., Kosaka, Y., Mauritsen, T., & Tatebe, H. (2020). Enhanced warming constrained by past trends in equatorial Pacific sea surface temperature gradient. *Nature Climate Change*, *11*, 33–37. doi:

10.1038/s41558-020-00933-3

Watanabe, M., Kamae, Y., Yoshimori, M., Oka, A., Sato, M., Ishii, M., … Kimoto, M. (2013, 6). Strengthening of ocean heat uptake efficiency associated with the recent climate hiatus. *Geophysical Research Letters*, *40*(12), 3175–3179. Retrieved from `https://agupubs.onlinelibrary.wiley.com/doi/full/10.1002/grl.50541https://agupubs.onlinelibrary.wiley.com/doi/abs/10.1002/grl.50541https://agupubs.onlinelibrary.wiley.com/doi/10.1002/grl.50541` doi: 10.1002/grl.50541

Wills, R. C. J., Dong, Y., Proistosecu, C., Armour, K. C., & Battisti, D. S. (2022, 9). Systematic Climate Model Biases in the Large-Scale Patterns of Recent Sea-Surface Temperature and Sea-Level Pressure Change. *Geophysical Research Letters*, *49*(17), e2022GL100011. Retrieved from `https://onlinelibrary.wiley.com/doi/full/10.1029/2022GL100011https://onlinelibrary.wiley.com/doi/abs/10.1029/2022GL100011https://agupubs.onlinelibrary.wiley.com/doi/10.1029/2022GL100011` doi: 10.1029/2022GL100011

Woodruff, S. D., Worley, S. J., Lubker, S. J., Ji, Z., Eric Freeman, J., Berry, D. I., … Wilkinson, C. (2011, 6). ICOADS Release 2.5: extensions and enhancements to the surface marine meteorological archive. *International Journal of Climatology*, *31*(7), 951–967. Retrieved from `https://onlinelibrary.wiley.com/doi/full/10.1002/joc.2103https://onlinelibrary.wiley.com/doi/abs/10.1002/joc.2103https://rmets.onlinelibrary.wiley.com/doi/10.1002/joc.2103` doi: 10.1002/JOC.2103

Wu, M., Zhou, T., Li, C., Li, H., Chen, X., Wu, B., … Zhang, L. (2021, 11). A very likely weakening of Pacific Walker Circulation in constrained near-future projections. *Nature Communications 2021 12:1*, *12*(1), 1–8. Retrieved from `https://www.nature.com/articles/s41467-021-26693-y` doi: 10.1038/s41467-021-26693-y

Yu, B., & Zwiers, F. W. (2010, 3). Changes in equatorial atmospheric zonal circulations in recent decades. *Geophysical Research Letters*, *37*(5), 5701. Retrieved from `https://onlinelibrary.wiley.com/doi/full/10.1029/2009GL042071https://onlinelibrary.wiley.com/doi/abs/10.1029/2009GL042071https://agupubs.onlinelibrary.wiley.com/doi/10.1029/`

2009GL042071 doi: 10.1029/2009GL042071

Yue, S., & Wang, C. (2002, 6). Applicability of Prewhitening to Eliminate the Influence of Serial Correlation on the Mann-Kendall Test. *Water Resources Research - WATER RESOUR RES*, *38*(6), 1–4. Retrieved from https://agupubs.onlinelibrary.wiley.com/doi/full/10.1029/2001WR000861 doi: 10.1029/2001WR000861

Zaplotnik, Z., Pikovnik, M., & Boljka, L. (2022, 3). Recent Hadley circulation strengthening: a trend or multidecadal variability? *Journal of Climate*, *-1*(aop), 1–65. Retrieved from https://journals.ametsoc.org/view/journals/clim/aop/JCLI-D-21-0204.1/JCLI-D-21-0204.1.xml doi: 10.1175/JCLI-D-21-0204.1

Zhang, L., & Karnauskas, K. B. (2017, 1). The Role of Tropical Interbasin SST Gradients in Forcing Walker Circulation Trends. *Journal of Climate*, *30*(2), 499–508. Retrieved from https://journals.ametsoc.org/view/journals/clim/30/2/jcli-d-16-0349.1.xml doi: 10.1175/JCLI-D-16-0349.1

Zhao, X., & Allen, R. J. (2019, 4). Strengthening of the Walker Circulation in recent decades and the role of natural sea surface temperature variability. *Environmental Research Communications*, *1*(2), 021003. Retrieved from https://iopscience.iop.org/article/10.1088/2515-7620/ab0dabhttps://iopscience.iop.org/article/10.1088/2515-7620/ab0dab/meta doi: 10.1088/2515-7620/AB0DAB

Indices of Pacific Walker Circulation strength: trends, correlations and uncertainty

K. Kosovelj[1], Ž. Zaplotnik[1,2], N. Žagar[3]

[1]Faculty of Mathematics and Physics, University of Ljubljana, Ljubljana, 1000, Slovenia
[2]European Centre for Medium-Range Weather Forecasts, Bonn, Germany
[3]Meteorological Institute, Center for Earth System Research and Sustainability, Universität Hamburg, 20146 Hamburg, Germany

Key Points:

- The evolution and trends of the Pacific Walker circulation (PWC) are evaluated using ten PWC indices in ERA5 data in the 1951-2020 period.
- Trends are strongly affected by the choice of representative time period and are rarely statistically significant.
- Positive and negative trends are suggestive of the presence of a multidecadal oscillation in the PWC.

Corresponding author: Katarina Kosovelj, katarina.kosovelj@fmf.uni-lj.si

Abstract

The strength of Pacific Walker circulation (PWC) significantly affects the global weather patterns, the distribution of mean precipitation, and modulates the rate of global warming. Different indices have been used to assess the PWC strength. Evaluated on different datasets for various study periods, the indices show large discrepancies between the reported trends. In this study, we performed sensitivity analysis of 10 PWC indices and compared them over the 1951-2020 period using the ERA5 reanalyses.

The time series of normalised indices generally agree on the annual-mean PWC strength. The highest correlations (exceeding $r = 0.9$) are between the indices that describe closely linked physical processes.

The trends of PWC strength are strongly affected by the choice of representative time period. For the commonly used 1981-2010 period, the trends show strengthening of the PWC. However, trends computed for longer period (i.e. 1951-2020) are mostly neutral, whereas the past two decades (2000-2020) display weakening of the PWC, although it is statistically not significant. The temporal evolution of trends suggests multidecadal variability of PWC strength with a period of about 35 years, implying a continued weakening of the PWC in the next decade.

Plain Language Summary

The Pacific Walker circulation (PWC) is tropical atmospheric circulation that consists of easterly winds close to the ground, westerlies aloft, upward motion in the western and downward motion over the eastern Pacific. The PWC impacts the rate of global warming and the sea-level rise. Thus, its accurate representation and prediction is an ultimate goal of climate models.

Towards this goal, the PWC strength has been described by a number of indices. Evaluated on different datasets and for various study periods, the PWC indices show large discrepancies between the reported trends. We assessed (dis)agreement among 10 PWC indices for 1951-2020 period using the ERA5 dataset, as the most reliable representation of the climate system since 1950. The indices computed from ERA5 data verify well with observations.

Indices generally agree on time series of PWC strength, with the highest correlations between the indices based on closely linked physical processes. However, we show

that the PWC trends are strongly affected by the choice of representative time period and often not statistically significant. They overall suggest weakening of PWC in the last two decades. Moreover, oscillatory structure of the trends suggest the presence of multidecadal oscillation of PWC.

1 Introduction

The Pacific Walker circulation (PWC) is the zonal part of the overturning tropical Pacific circulation, driven by the zonal pressure gradient and associated with the longitudinal gradients of sea-surface temperature. The PWC is characterized by the ascending motion over the warmer western Pacific east of around 150°E, and descending motion over the cooler eastern Pacific west of around 90°W (Peixoto & Oort, 1992; Seager et al., 2019). The circulation cell is completed by the upper-tropospheric equatorial westerlies and lower-tropospheric equatorial easterlies. The magnitude of the involved horizontal and vertical motions defines the PWC strength.

The strength of PWC is largely synced with the Pacific ocean circulation via the Bjerknes feedback (Bjerknes, 1969). Thus, it crucially impacts the global climate; it affects the precipitation distribution in the tropics (e.g., Barichivich et al., 2018) as well as in extratropics via atmospheric teleconnections, it is coupled to the mean-sea level in the tropical Pacific (e.g., Merrifield, 2011; Muis et al., 2018), impacts heat uptake (e.g., Meehl et al., 2011; England et al., 2014; McGregor et al., 2014), carbon uptake and carbon outgassing (Betts et al., 2020) and therefore also the rate of climate-change-induced warming in tropics and extratropics, particularly in winter when the heat-transporting stationary/transient eddies are stronger (Kosaka & Xie, 2013). Therefore, a comprehensive description and accurate prediction of PWC is of great societal importance.

Several distinct metrics have been used in the literature to date to describe the PWC strength and its changes in time. These metrics have been applied to distinct observational and reanalysis datasets for distinct time periods. For example, Sohn and Park (2010) related the PWC strength to the magnitude of the water vapor transport in the lower return branch of PWC. Using satellite data (from microwave imager and infrared sounder) and reanalyses, they reported a PWC strengthening in the 1979-2007 period. Similar conclusions were reached by Sohn et al. (2013) for the 1979-2008 period using purely observational datasets and different metrics including sea-surface-temperature (SST) and sea-level-pressure (SLP) differences across the equatorial Pacific. Kociuba and Power (2015) applied an identical SLP index and observed significant strengthening in the 1980-2012 period, whereas any trend starting before 1951 and ending in 2012 is negative. Strengthening of the PWC in recent decades was suggested also by Chen et al. (2008); Luo et al. (2012); Meng et al. (2012); L'Heureux et al. (2013); Bayr et al. (2014); Sandeep et al. (2014); Chung et al. (2019); Zhao and Allen (2019), as well as by the isotopic analysis of δ^{18}O (Falster et al., 2021). The PWC strengthening in turn lead to increased zonal sea-surface temperature (SST) gradients in the equatorial Pacific (Seager et al., 2019), and enhanced upwelling of the cold deep-ocean water in the Eastern Pacific, causing the so-called global warming hiatus in the 2000s and early 2010s (Kosaka & Xie, 2013; England et al., 2014; Watanabe et al., 2013).

In contrast, a number of studies reported a weakening trend of PWC, in particular for indices evaluated using numerical modeling. Bellomo and Clement (2015) related the vertical velocity in the PWC's ascending branch to the observed cloud cover and argued for a weakening PWC trend for the 1954-2008 period, consistent with the projected weakening by the climate models due to anthropogenic climate change (Knutson & Manabe, 1995; Held & Soden, 2006; Vecchi et al., 2006; Vecchi & Soden, 2007; Bayr et al., 2014; Wu et al., 2021; Masson-Delmotte et al., 2021). PWC weakening between 1950 and 2009 has been also suggested by Tokinaga et al. (2012) who analyzed the SLP gradient over the tropical Pacific derived from the atmospheric general circulation model (AGCM) experiments forced by the SSTs from the International Comprehensive Ocean–Atmosphere Data Set (ICOADS, Woodruff et al., 2011), instead of the more commonly used HadISST1 data (Rayner et al., 2003). Other studies reporting a weakening trend of the Walker circulation in the 20th century include Deser et al. (2010), Power and Kociuba (2011) and DiNezio et al. (2013). This was supported by the isotopic analysis of corals in the tropical Pacific (Liu et al., 2019).

The examples above reveal opposite conclusions about the trends of PWC strength using different datasets and metrics of PWC strength. The PWC time series reflect a combination of forced signal and multidecadal climate variability, making a direct intercomparison of various studies difficult, even for largely-overlapping periods. While a strengthening of the PWC in the period after 1979 seems firmly established (Wu et al., 2021), its near-future projection is less clear. It is necessary to systematically intercompare the PWC indices in use and their sensitivity to the analysis periods for the computation of the trends. We carry out such a comparison in this paper. The paper complements previous studies by L'Heureux et al. (2013), Plesca et al. (2018) and Chung et al. (2019) that compared the PWC trends for several PWC indices, by performing a systematic intercomparison of ten PWC indices used in the literature up to date on the latest generation of the European reanalyses, ERA5.

We evaluate the ten indices using the ECMWF ERA5 dataset in the 1951-2020 period (Hersbach et al., 2020), we test their sensitivity to averaging regions and levels, and verify them with their equivalents derived directly from observations. The definitions of 10 indices and details about various datasets are provided in Section 2. The time series of PWC indices, their correlations, and the sensitivity of the derived trends to different periods are compared in Section 3. Conclusions and discussions are given in Section 4.

2 Pacific Walker Circulation Indices and Datasets

We present ten indices, that are considered suitable given results from their recent applications and understanding of tropical east-west circulation.

2.1 Definitions of Indices

The following indices of Pacific Walker Circulation are compared:

1. Point-based Southern oscillation index (SOI) from Troup (1965), which is defined by the anomaly in the mean sea-level pressure difference between Tahiti and Darwin station data standardized for each month of the year using 1950-2021 as a base period. As we compute the SOI from the reanalysis data, the closest model gridpoints are used for evaluation (see Supplementary Information Fig. S1 for justification).

2. Area-averaged Southern oscillation index ΔSLP from Vecchi et al. (2006), defined as a difference between anomalies in mean sea-level pressure over the eastern and western equatorial Pacific. The anomalies are averaged over two boxes, both extending from 5°S to 5°N in meridional directions. In zonal direction the boxes extend from 80°E to 160°E (western Pacific box) and from 80°W to 160°W (eastern Pacific box). This index has been widely used due to the availability of long-term historical data on sea-level pressure.

3. Velocity potential index from Tanaka et al. (2004) that is computed for 2D circulation at a single vertical level (typically pressure p level) by solving the Poisson equation

$$\nabla \cdot \mathbf{V}_p = -\nabla^2 \chi_p. \tag{1}$$

The index was originally defined by Tanaka et al. (2004) as the yearly average of maximum deviation of velocity potential from its zonal mean over equatorial Pacific at 200 hPa level, χ_{200}. Here, the yearly averaging was applied as a 12-month running mean. However, as the maximum divergent outflow from a convective area over the Maritime continent is higher up in the troposphere (see Fig. S2) and varies year-to-year, we rather constructed a data-adaptive index $\chi_{\max}$, which takes the maximal velocity potential over equatorial Pacific at each time step (see Section 3 for argumentation and Fig. S3 for justification).

4. Vertical velocity index from Wang (2002) (named ω_{500}), calculated as the difference in average vertical pressure velocity anomalies between eastern and western equatorial Pacific at 500 hPa. Eastern Pacific is defined as an area between 120°W and 160°W, and from 5°S to 5°N). The Western Pacific is defined between 120°E and 160°E, and from 5°S to 5°N).

5. The sea-surface temperature (SST) index defined the same way as the ΔSLP index, but for the SST data. SST data are often used as a proxy/driver for PWC strength (Tokinaga et al., 2012; Meng et al., 2012; Zhang & Karnauskas, 2017).

6. Effective wind for water vapor transport index following Sohn and Park (2010). The boundary layer easterlies in the lower return branch of the Walker circulation carry the water vapor from the eastern to the western Pacific to provide additional fuel for condensation heating, which maintains the Walker circulation. The increase and decrease of water vapor flux, normalized by the total amount of vapor in the atmospheric column, is regarded as the strengthening and weakening of circulation, respectively. The effective wind is defined as:

$$\mathbf{V}_e = \sum_{i=1}^{N} \frac{PW\left(i\right)}{TPW} \mathbf{V}_D\left(i\right), \tag{2}$$

where PW(i) is precipitable water in a vertical layer between i-th and i + 1-th vertical level, TPW is the total precipitable water in a column and $\mathbf{V}_D\,(i)$ is divergent wind at i-th vertical level. The summation goes from the ground level upwards (in our case from 1000 hPa to 850 hPa).

Precipitable water $PW\,(i)$ is calculated as

$$PW\,(i) = \frac{1}{\rho_w g} \int_{p_i}^{p_{i+1}} q\,(p)\,\mathrm{d}p, \tag{3}$$

where ρ_w is water density, g is gravity acceleration, $q\,(p)$ is specific humidity, and p_i and p_{i+1} are boundaries of specific layer ($p_{i+1} < p_i$). Total precipitable water is calculated in the same way, with $p_i = p_s$ (surface pressure) and p_{i+1} is at the top of the atmosphere.
As we are interested in Walker circulation, we only used the zonal component of the divergent wind (u_D) and defined the index (named V_e) as an average value of effective zonal wind for water vapor transport in the tropical Pacific area (120°E to 120°W, and 5°S to 5°N).

7. Stream function index, based on a mass stream function:

$$\psi\,(p) = \frac{2\pi a}{g} \int_0^p u\,\mathrm{d}p, \tag{4}$$

where a is the radius of the Earth, g is gravity acceleration, and u is the zonal component of wind averaged between 5°S and 5°N. We define the index (named ψ_{500}) as maximal stream function at 500 hPa within 90°E and 80°W. Originally this index was defined using the zonal component of divergent wind (Yu & Zwiers, 2010; Bayr et al., 2014). Whereas the divergent circulation explains the majority of the meridional tropical circulation (Pikovnik et al., 2022), the zonal response to deep convective forcing over the Maritime continent projects on both the rotational and divergent flows (Gill, 1980). Thus, we opted for the zonal component of the total wind instead of its divergent part (their difference is shown in Fig. S4).

8. Zonally-integrated (across the Pacific basin) wind stress following Clarke and Lebedev (1996), i.e. L_τ. It is defined as

$$L_\tau = \int_0^L \overline{\tau_x}\mathrm{d}x, \tag{5}$$

where $\overline{\tau_x}$ is meridionally averaged zonal wind stress. Zonal integration is performed between 124°E and 90°W. In the meridional direction, we choose to average between 5°S and 5°N, to be consistent with other indices. Following Clarke and Lebedev (1996), we computed wind stress as

$$\tau_x = \rho_a c_D \left|\mathbf{V}\right| u, \tag{6}$$

where ρ_a is air density (with a constant value of 1.2 kg/m^3 as in Clarke and Lebedev (1996)), c_D is drag coefficient (1.5×10^{-3}), and $\mathbf{V}$ is horizontal surface wind vector at 10 m elevation ($\mathbf{V} = (u, v)$).

9. Upper tropospheric specific humidity (denoted Q_{200}). As the upper-tropospheric water vapor in the western equatorial Pacific is mainly transported by deep convection in the ascending branch of the PWC, a change in the upper-tropospheric humidity may indicate a change in the circulation strength (Sohn et al., 2013). To eliminate the increase of specific humidity (a general increase in humidity due to global atmospheric warming), we formulated the index as the difference in upper tropospheric humidity at the top of ascending and descending branches of Walker circulation. The humidity Walker circulation index is then defined as a difference in average specific humidity between two boxes over the eastern and western Pacific at 200 hPa. We used the same horizontal boxes for specific humidity as they were used for ω_{500}.

10. Average surface zonal winds over the central equatorial Pacific (denoted U_{ave}), after Chung et al. (2019). The index is applied by averaging 10 m wind over an area from 6°S to 6°N and from 180° to 150°W.

The ten indices can be grouped into two categories: (a) the direct circulation indices ($\chi_{\max}$, ψ_{500}, L_τ, U_{ave}, $\mathbf{V}_e$ and ω_{500}) which directly measure the velocity of the flow or associated flow function in any of the PWC branches, and (b) the indirect indices of the PWC magnitude derived from the atmospheric mass field or the lower boundary (Q_{200}, SOI, ΔSLP and SST). The Q_{200} index measures PWC strength through the convective humidity-influx in the upper troposphere, whereas the SST index measures the PWC strength through coupled ocean-atmosphere interactions.

All indices are influenced also by other parts of the tropical general circulation, i.e. by the Hadley and Monsoon circulations. In particular, indices that indirectly measure PWC strength and may not only be representative of the PWC changes but also of the accompanying local Hadley cells (Sohn et al., 2019; Pikovnik et al., 2022; Zaplotnik et al., 2022). The anthropogenic warming of the atmosphere and increasing water content directly affect the thermodynamic indices, whereas the SST index is also affected by the ocean processes.

Some of the indices attain physical units, some are made dimensionless, and they may have largely different magnitude. To make indices comparable, we standardize them, i.e. the mean value of the index is subtracted from each index and then normalized by its standard deviation within the study period. All indices are computed for 1950-2021 period. As application of running mean shortens time series of χ indices for six month at each end of the interval, the comparison of indices is performed on 1951-2020 period.

The indices require different amounts of data for their evaluation. SOI is calculated from pressure in two particular locations and can be affected by the local microclimate, especially when computed from station measurements, whereas indices from area-averaged data (ΔSLP, ω_{500}, SST, $\mathbf{V}_e$, L_τ, Q_{200}, U_{ave}) should better represent large processes. Some of the indices require only one basic variable and are easily calculated (e.g. SOI, ΔSLP, SST, Q_{200}, U_{ave}), while others require derived products (e.g. ψ_{500}, χ_{max}, L_τ, $\mathbf{V}_e$) and/or more complex calculation (e.g. ψ_{500}, $\mathbf{V}_e$). It is therefore logical that historically, the choice of the PWC index was influenced by the availability of data and computational resources.

2.2 Data

To intercompare a range of PWC indices, a dataset based on fully-coupled atmosphere-ocean modeling is required. The latest ERA5 reanalysis data are used for the period 1950-2021 (Hersbach et al., 2020, 2018a; Bell et al., 2020a). The indices are derived from the pressure vertical velocity ω, the zonal and meridional winds and specific humidity, which are provided on a regular latitude-longitude grid with 1° horizontal resolution and 27 vertical pressure levels, extending from 100 to 1000 hPa. Sea surface temperature (SST) data and the mean-sea-level pressure (MSLP) data are at the same horizontal grid (Hersbach et al., 2018b; Bell et al., 2020b). Depending on the index, we use either monthly means, computed from either daily 00 UTC data for horizontal winds (u and v) or daily means for all other variables (MSLP, ω, specific humidity q, and sea-surface temperature SST). The mixed-use of 00 UTC and daily mean data was justified by comparison of both datasets for the ωindex at 500 hPa, as the ω is one of the variables most affected by the diurnal cycle. However, the choice of 00 UTC or daily mean data has negligible impact on the indices (see Fig. S5).

We consider ERA5 sufficient for the analysis for several reasons. First, Simmons (2022) has shown that ERA5 very well verifies with the upper-tropospheric wind measurements in the tropics. The mean departure between the observations and background or first-guess in data assimilation (i.e. short-range forecasts) for upper-tropospheric zonal winds is trend-free and less than 1 m/s from the late 1990s onwards. In addition, the supplemental material includes our verification of PWC indices based on surface winds in ERA5 and the Wave- and Anemometer-based Sea surface wind product (WASWind, Tokinaga & Xie, 2011) showing their close correspondence (Fig. S6). Similarly, the ERA5-derived SST indices agree well with the indices derived from HadISST data (Rayner et al. (2003); see Fig. S7 for comparison). The same applies to the SOI index based on ERA5 data verified against the index derived from raw station data (Fig. S1).

3 Results

In this section we first discuss temporal evolution of the ten indices (including their reformulations in two cases) and correlation coefficients between various indices. This is followed by the evaluation of trends and their sensitivity to the period used for the computation of the trends.

3.1 Time-series of PWC indices and their correlations

Time series of the normalised annual-mean PWC indices (Fig. 1a) agree relatively well on the evolution and relative strength of PWC during most of the period since 1950. The majority of the indices spot strong El Niños in e.g. 1972, 1982/83, 1987, 1992, 1997/98, and 2015. There is more discrepancy between the indices regarding La Niñas, as they tend to be more prolonged. The two indices that deviate most from the others are the stream function index based on the divergent zonal wind at 500 hPa and velocity potential at 200 hPa. Their more poor agreement with other indices motivated their reformulation as described in the previous section and discussed below.

The fact that different indices describe different aspects of PWC implies that their correlations will vary (Fig. 1b). Correlations are generally high between the indices derived from physically linked processes. For example, the pair of indices with the high-

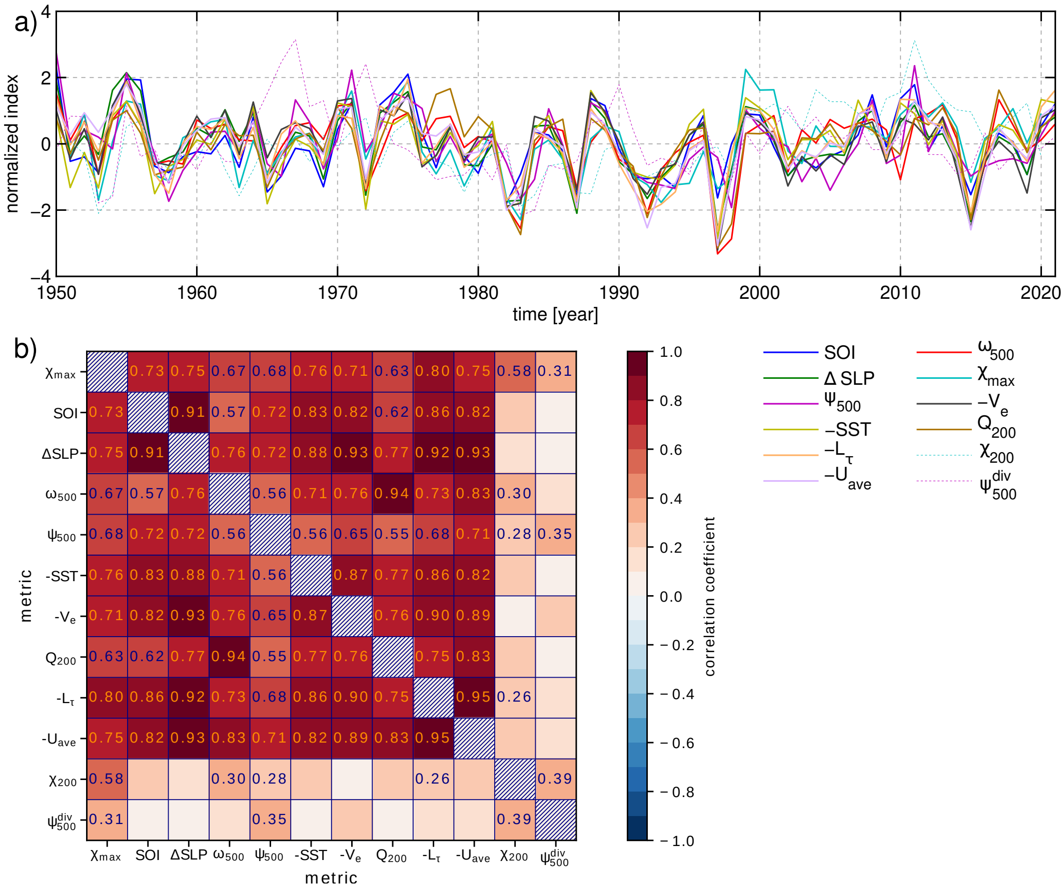

Figure 1. a) Time series of annual-mean PWC strength in ERA5 reanalysis between 1950 and 2021 for different PWC indices described in Section 2.1 as shown in the legend. b) Correlations between annual means of different PWC indices. Statistically significant (at 95 % confidence level) correlation coefficients are written in the respective fields. SST, V_e, L_τ and U_{ave} indices are multiplied by (-1) for easier comparison with other indices. χ_{200} and ψ_{500}^{div} are shown dashed in a) as they are replaced by better defined equivalent indices and not used in the continuation.

est correlation coefficient ($r = 0.95$) is U_{ave} and L_τ, which both describe surface easterlies. The ω index very highly correlates ($r = 0.94$) with the Q-index, as the amount of upper tropospheric humidity is directly related to the magnitude of vertical water vapor transport through convection. Similarly, the ΔSLP index correlates very highly ($r =$ 0.92 to 0.93) with the zonal surface wind index U_{ave}, surface wind stress index L_τ, and zonal boundary-layer moisture transport (represented by the effective wind V_e). This can be expected, as the pressure difference (expressed by SOI, ΔSLP) over the Pacific drives the near-surface equatorial easterlies. The larger the pressure difference, the stronger the easterlies (U_{ave}), the wind stress (L_τ), and the water vapor transport (V_e).

The correlations are somewhat lower between indices derived from distinct processes, e.g. surface wind and upper-tropospheric humidity ($r = 0.83$). Moderate correlations are observed between ω, and SST and ΔSLP indices with $r = 0.71$ and 0.76, respectively. This suggests, that the convective mass flux over the Maritime continent is controlled not only by the zonal SST gradient or SLP gradient but also by the local meridional gradients in the Western Pacific (Sohn et al., 2019). This is further supported by a rather moderate correlation ($r = 0.56$) between the SST and ψ indices, suggested also by He et al. (2014).

The original χ_{200} index (Tanaka et al., 2004) and stream-function index ψ_{500}^{div} (Yu & Zwiers, 2010; Bayr et al., 2014) (both indicated with dashed line in Fig. 1a) stand out from the rest and do not properly distinguish between the strongest El Niños. After the year 2000, χ_{200}-index also significantly exceeds the values of other indices. The velocity-potential index is highly susceptible to the choice of upper-tropospheric pressure level, in connection to the strong vertical profile of the divergent outflow (see Figs. S2, S3). The peak divergent outflow also occurs at different pressure levels year-to-year. Therefore an index defined at some predetermined pressure level can miss peak velocity potential. To alleviate it, we constructed a data-adaptive index, which takes the maximum of monthly-mean χ at any level within the box area. Such index correlates almost perfectly with the χ_{150} index ($r = 0.98$), meaning that the original χ_{200} index was applied too low in the troposphere. Our reformulated index χ_{max} verifies much better with other PWC indices (Fig. 1b).

Similarly, the stream-function index computed from total zonal wind instead of the zonal divergent wind verifies well with other PWC indices. The original stream-function index based on the divergent wind deviates from other indices in particular in the pre-satellite era in the 1960s and 1970s (see Figs. 1a and S8). Correlations with other indices are small, and the only statistically significant correlations for annual means are with χ_{200}, $\chi_{\max}$ and ψ_{500} indices (r between 0.3 and 0.4).

PWC indices are typically defined at fixed vertical levels where the underlying physical processes are on average the strongest; for example, the divergent outflow is strongest in the upper troposphere at around 150 hPa level (Fig. S2) and the stream function has largest amplitude at 500 hPa level. As the PWC strength and position oscillate on a year-to-year basis, the intercomparison of PWC indices might be skewed due to the displacement of maxima from vertical levels on which indices are computed. To ensure that our results are not significantly affected by such displacements, we tested the sensitivity of the indices to meaningful changes in the choice of the vertical level. The sensitivity was checked for χ, ω, ψ, and Q indices (see Figs. S3, S5, S8, and S9). We also checked the sensitivity of indices to different meridional extents of horizontal areas used in their computation (see Fig. S8 for ψ and Fig. S9 for Q-index). As the tropical processes are mainly centered at the ITCZ, we checked how the indices, originally defined in a narrow equatorial belt (5°S and 5°N) change when meridional borders of the areas considered were modified (5°N and 20°N) to better align with the average position of ITCZ. This was applied to V_e, ψ, L_τ, and Q indices. In general, the indices are not very sensitive to the vertical level or horizontal area used for calculation, as long as the chosen level/area is close to the level/area used in the original definition. This is supported by high correlation coefficients between different variations of each index (not shown). The only exception is the χ index, which varies significantly with the vertical level used for computation, as already mentioned. Our sensitivity analysis confirms that the results on PWC changes, presented in this paper, are not meaningfully impacted by the mild shifts of vertical levels or meridional averaging.

3.2 Trends in PWC and their sensitivity to the WC

The PWC trends are evaluated from time series of standardized annual-mean PWC indices using linear regression. Figure 2 shows trends computed starting from various years from 1951 to 2000, with the end year of the interval fixed to 2020. This figure shows that the trends depend on the starting year. Most indices show neutral-to-negative trends for the start year between 1951 and 1970, suggesting that PWC has remained steady or has been slightly weakening in the recent 70-year or 50-year time period. The exceptions to this rule are the velocity-potential index and the SST index, which show strengthening of PWC until nearly the end of 20th century. In the 1980-2020 period, the PWC has been strengthening according to most of the PWC indices. However, only $\chi_{\max}$, ω_{500} and L_τ indices show statistically significant strengthening at the 95% confidence level according to the modified, trend free, pre-whitening Mann-Kendall test (Yue & Wang, 2002; Hussain & Mahmud, 2019) (see Table S1). This applies also to the 1990-2020 period with one half of the indices showing statistically significant trends. In the recent two decades (2000-2020 period), the majority of the indices suggests PWC weakening, although the uncertainty is relatively large.

Next question to ask is how the trends vary if both the end and start year for the computation of the trend vary. This is shown in Fig. 3. Three distinct areas can be identified in the figure, although not equally clear for all ten indices: 1) trends, starting in the 1950s, and ending in the 1970s are mostly positive, suggesting an increase in PWC strength; 2) trends, starting approximately between 1960 and 1980, and ending around 2010 are mostly negative and often statistically significant, suggesting a weakening of PWC; 3) trends, starting between around 1980 and mid to late 1990s are again mostly positive, regardless of the end year. On the other hand, long-term trends starting before the mid-1970s and ending after the year 2010 are insignificant and have even different signs.

The right diagonal line shows 20-year running trends with start years from 1951 to 2000. This suggests approximately 20 years of downtrend (blue colours, start years 1963 to 1980) followed by 20 years of uptrend (red colours, start years 1980 to 1997). Together, this suggests a multidecadal variability of the PWC with an approximately 35-year period. If so, blue patches in the upper-right corners of Fig. 3, that indicate a PWC weakening, together with recent trends in Fig. 2 suggest that a multidecadal trend reversal might be just taking place. Although a further analysis with longer dataset is needed to confirm that the trends are associated with a multidecadal oscillation in PWC, our expectation of a weakened PWC in the coming years agree with Wu et al. (2021) who reached their conclusion by coupling the PWC with the Interdecadal Pacific Oscillation.

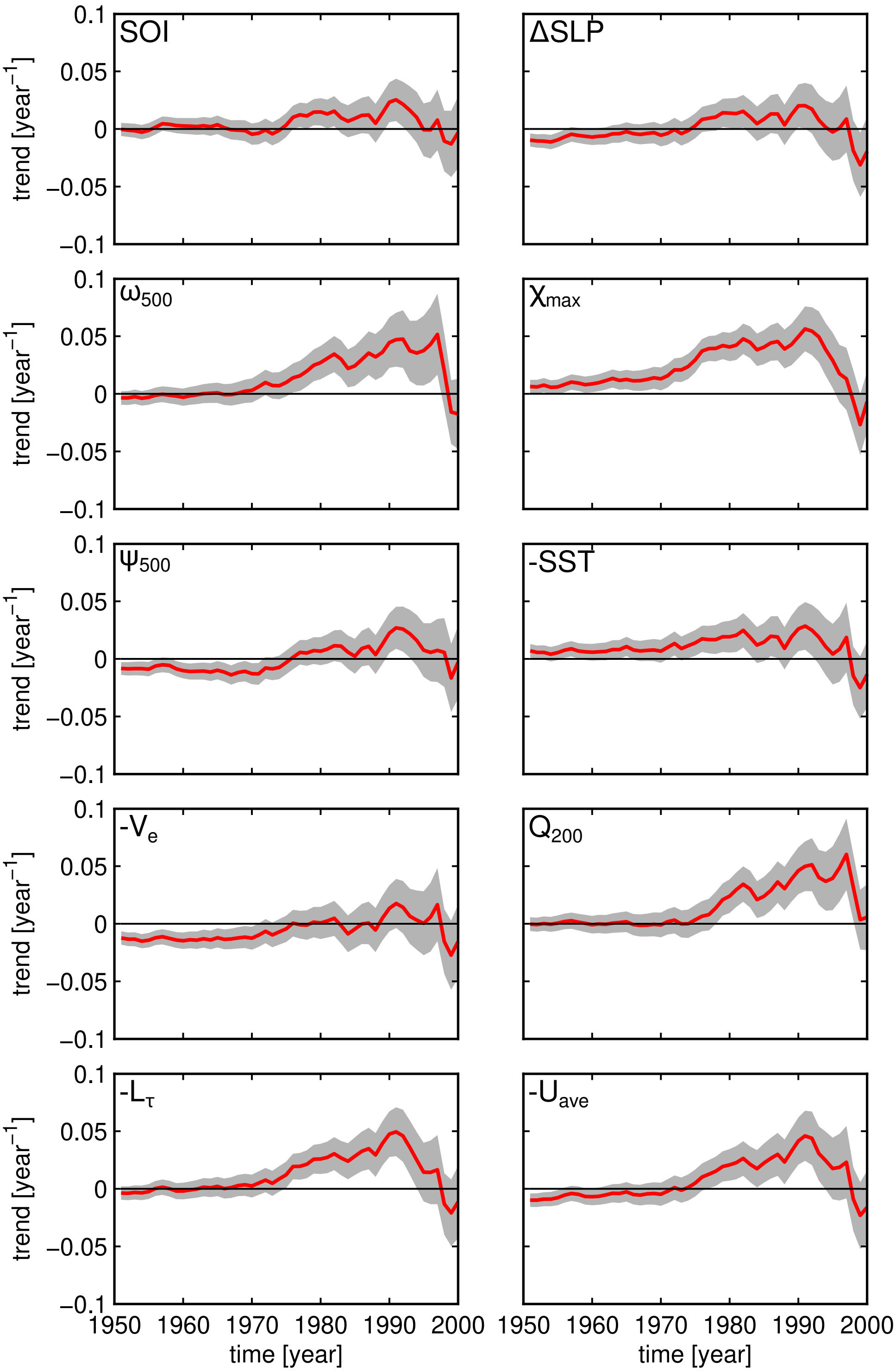

Figure 2. Trends of Pacific Walker circulation (PWC) strength as a function of the starting year of the trend for different PWC indices. The end year of all linear trends is fixed to 2020. For example, the year 1970 on the x-axis represents the PWC trend calculated for 1970-2020. PWC trends for periods shorter than 20 years are not shown. Thick red lines represent the trend value, and the gray areas represent the uncertainty (i.e. plus or minus one standard deviation) of the estimated trend. SST, V_e, L_τ and U_{ave} indices are multiplied by (-1) for easier comparison with other indices.

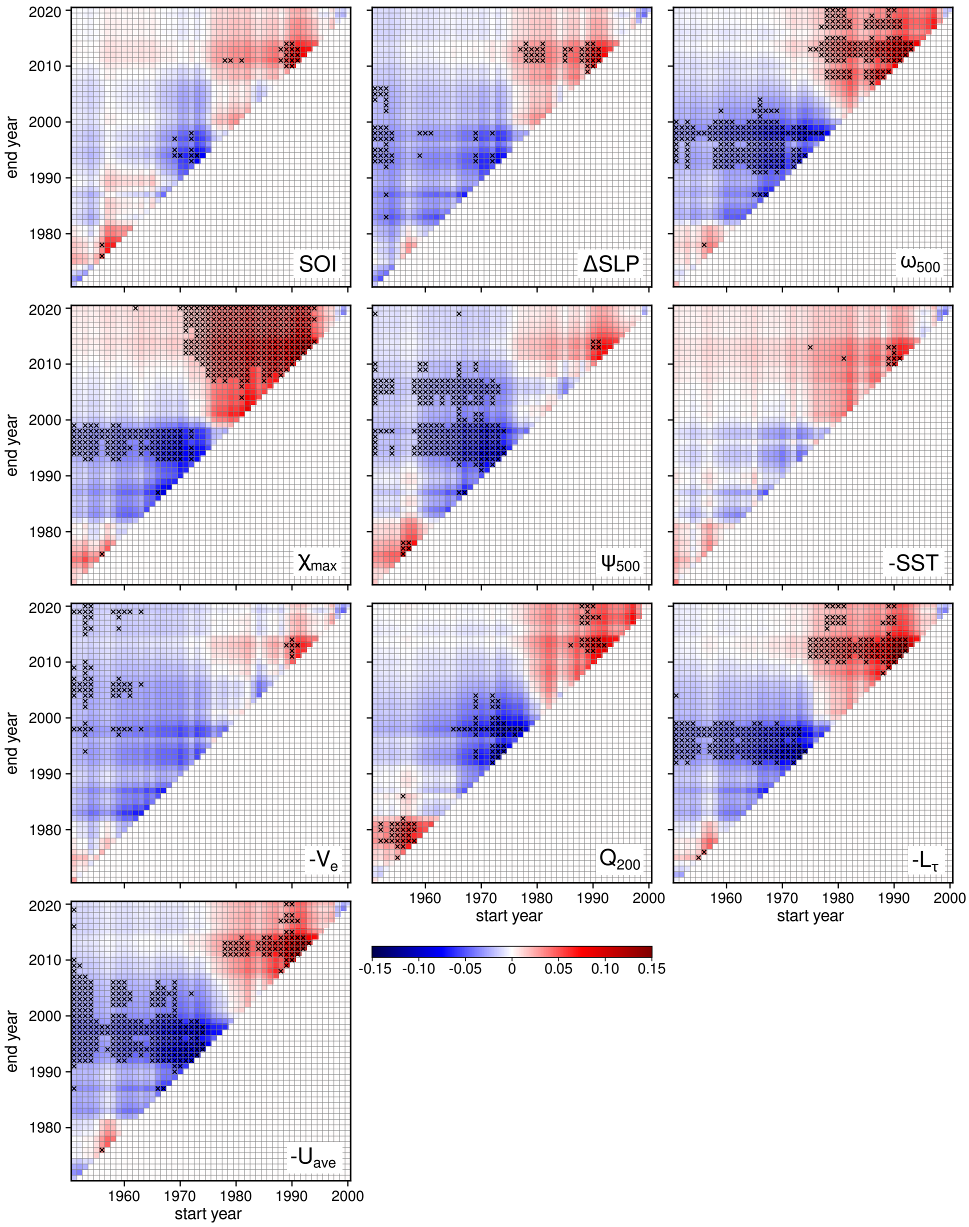

Figure 3. Trends of Pacific Walker circulation (PWC) strength as a function of the starting year (x-axis) and end year (y-axis) of the trend for different PWC indices. PWC trends for periods shorter than 20 years are not shown. Crosses represent statistically significant trends at the 95% confidence level. SST, V_e L_τ and U_{ave} indices are multiplied by (-1) for easier comparison with other indices. The checkered pattern is a result of ENSO variability. First row in the matrix is a realisation of Fig. 2. The bottom-left top-right diagonal (0-diagonal) effectively represents a 20-year running trend (as in e.g. L'Heureux et al., 2013), whereas the k-diagonal represents a $(20 + k)$-year running trend.

4 Discussion and Conclusions

The study compares ten different indices of the Pacific Walker circulation (PWC) strength over the 1951-2020 period using the ECMWF ERA5 reanalyses. We have shown that the indices derived from ERA5 are equivalent to indices deduced from the raw observation data, as ERA5 accurately verifies with the observations of upper-tropospheric zonal winds, zonal surface winds, sea-level pressure, sea-surface temperature (see Supplementary information and Hersbach et al., 2020; Simmons, 2022). Some PWC indices have been refined. For example, the χ index was originally defined at 200 hPa (Tanaka et al., 2004). However, the newest state-of-the-art datasets suggest that the maximum divergent outflow associated with convection over the western Pacific is higher in the troposphere, at around 150 hPa. Similarly, the original definition of the stream function index is based on divergent wind (Yu & Zwiers, 2010; Bayr et al., 2014) and appears to miss an important part of the zonal tropical circulation associated with the PWC. Thus, we suggest to replace χ_{200} and ψ_{500} by $\chi_{\max}$ and $\psi_{500}^{\mathrm{tot}}$, respectively.

In general, the normalized PWC indices agree regarding the variation of annual-mean PWC strength (see Fig. 1a). The correlations are highest ($r = 0.9$ or more) between the indices which describe closely linked processes, as could be expected. The indices are most often based on a single level. We have shown that the sensitivity of indices to the reasonable changes in the choice of vertical level or horizontal averaging area is negligible. One exception is the velocity potential index, which displays strong sensitivity to the choice of vertical level.

The sensitivity of the trends to the applied periods is often poorly explored in the literature. Our study shows that different indices, different lengths of the applied interval, and their start and end years, can largely affect the trends and their significance. In the common climatological reference period 1981-2010, the majority of indices showed PWC strengthening. On the longer time scales, i.e. 1951-2020, the trend is mostly neutral and insignificant. Furthermore, the majority of indices suggest that the PWC might have been weakening during the last two decades (2000-2020). A continuation of this trend implies a reversal of the PWC into an El Niño-type state with decreased ocean heat uptake and more rapid global warming. We suggest that the observed variability in the trends of the PWC indices is associated with the multidecadal variability of the PWC with a period of about 35 years. Longer data series are needed to confirm this result.

The recent (1981-2010) PWC strengthening has been unequivocally opposed to the climate model projections (Gulev et al., 2021). Whether the source of the discrepancy is multidecadal variability as seen in Fig. 3 (Meng et al., 2012; Chung et al., 2019; Wu et al., 2021), forced response (Mann et al., 2021; Orihuela-Pinto et al., 2022) or biases in the coupled ocean-atmosphere climate models (Durack et al., 2012; McGregor et al., 2014; Seager et al., 2019; Watanabe et al., 2020; Wills et al., 2022), caution should be exercised for the detection and comparison of PWC trends in the models and reanalyses. We speculate a shift toward weakening of the PWC. If realised, it will crucially impact the global distribution of precipitation in the tropics and extratropics, the ocean heat uptake (e.g. Meehl et al., 2011), the sea-level rise and the rate of global warming.

Appendix A Open Research

ERA5 data (https://doi.org/10.24381/cds.bd0915c6, Hersbach et al., 2018) was downloaded from the Copernicus Climate Change Service (C3S) Climate Data Store (last access 27 June 2022). The results contain modified Copernicus Climate Change Service information 2022. Neither the European Commission nor ECMWF is responsible for any use that may be made of the Copernicus information or data it contains.

Scripts for calculation of indices and data used to generate Figs. 1-3 and S1-S12 are published in Zenodo data repository: https://doi.org/10.5281/zenodo.7359879 (Kosovelj et al., 2022).

Acknowledgments

This research has been supported by the Javna Agencija za Raziskovalno Dejavnost RS (grant no. J1-9431 and Programme P1-0188). Research of Nedjeljka Žagar contributes to Germany's Excellence Strategy—EXC 2037 'CLICCS—Climate, Climatic Change, and Society'-project number: 390683824, contribution to the Center for Earth System Research and Sustainability (CEN) of Universität Hamburg.

The Authors thank Matic Pikovnik (Slovenian Environment Agency, ARSO, and University of Ljubljana, Faculty of Mathematics and Physics) for sharing parts of the code that contributed to this research.

References

Barichivich, J., Gloor, E., Peylin, P., Brienen, R. J., Schöngart, J., Espinoza, J. C., & Pattnayak, K. C. (2018). Recent intensification of Amazon flooding extremes driven by strengthened Walker circulation. *Science Advances*, *4*(9). Retrieved from https://www.science.org/doi/10.1126/sciadv.aat8785 doi: 10.1126/SCIADV.AAT8785/SUPPL{_}FILE/AAT8785{_}SM.PDF

Bayr, T., Dommenget, D., Martin, T., & Power, S. B. (2014). The eastward shift of the Walker Circulation in response to global warming and its relationship to ENSO variability. *Climate Dynamics*, *43*(9-10), 2747–2763. doi: 10.1007/s00382-014-2091-y

Bell, B., Hersbach, H., Berrisford, P., Dahlgren, P., Horányi, A., Muñoz Sabater, J., ... Thépaut, J.-N. (2020a). *ERA5 hourly data on pressure levels from 1950 to 1978 (preliminary version).* Copernicus Climate Change Service (C3S) Climate Data Store (CDS). Retrieved from https://cds.climate.copernicus-climate.eu/cdsapp#!/dataset/reanalysis-era5-pressure-levels-preliminary-back-extension?tab=overview

Bell, B., Hersbach, H., Berrisford, P., Dahlgren, P., Horányi, A., Muñoz Sabater, J., ... Thépaut, J.-N. (2020b). *ERA5 hourly data on single levels from 1950 to 1978 (preliminary version).* Copernicus Climate Change Service (C3S) Climate Data Store (CDS). Retrieved from https://cds.climate.copernicus-climate.eu/cdsapp#!/dataset/reanalysis-era5-single-levels-preliminary-back-extension?tab=overview

Bellomo, K., & Clement, A. C. (2015, 9). Evidence for weakening of the Walker circulation from cloud observations. *Geophysical Research Letters*, *42*(18), 7758–7766. Retrieved from https://onlinelibrary.wiley.com/doi/full/10.1002/2015GL065463https://onlinelibrary.wiley.com/doi/abs/10.1002/2015GL065463 doi: 10.1002/2015GL065463

Betts, R. A., Burton, C. A., Feely, R. A., Collins, M., Jones, C. D., & Wiltshire, A. J. (2020). ENSO and the Carbon Cycle. *Geophysical Monograph Series*, *253*, 453–470. Retrieved from https://onlinelibrary.wiley.com/doi/full/10.1002/9781119548164.ch20https://onlinelibrary.wiley.com/doi/abs/10.1002/9781119548164.ch20https://agupubs.onlinelibrary.wiley.com/doi/10.1002/9781119548164.ch20 doi: 10.1002/9781119548164.CH20

Bjerknes, J. (1969). Atmospheric Teleconnetions from the Equatorial Pacific. *Monthly Weather Review*, *97*(3), 163–172. Retrieved from https://journals.ametsoc.org/view/journals/mwre/97/3/1520-0493_1969_097_0163_atftep_2_3_co_2.xml doi: 10.1175/1520-0493(1969)097⟨0163:ATFTEP⟩2.3.CO;2

Chen, J., Del Genio, A. D., Carlson, B. E., & Bosilovich, M. G. (2008). The Spatiotemporal Structure of Twentieth-Century Climate Variations in Observations and Reanalyses. Part I: Long-Term Trend. *Journal of Climate*, *21*(11), 2611–2633. Retrieved from https://journals.ametsoc.org/view/journals/clim/21/11/2007jcli2011.1.xml doi: 10.1175/2007JCLI2011.1

Chung, E. S., Timmermann, A., Soden, B. J., Ha, K. J., Shi, L., & John, V. O. (2019). Reconciling opposing Walker circulation trends in observations and model projections. *Nature Climate Change*, *9*(5), 405–412. Retrieved from https://doi.org/10.1038/s41558-019-0446-4 doi: 10.1038/s41558-019-0446-4

Clarke, A. J., & Lebedev, A. (1996). Long-Term Changes in the Equatorial Pacific Trade Winds. *Journal of Climate*, *9*(5), 1020–1029.

Deser, C., Phillips, A. S., & Alexander, M. A. (2010). Twentieth century tropical sea surface temperature trends revisited. *Geophysical Research Letters*, *37*(10). Retrieved from https://onlinelibrary.wiley.com/doi/full/10.1029/2010GL043321 doi: 10.1029/2010GL043321

DiNezio, P. N., Vecchi, G. A., & Clement, A. C. (2013). Detectability of Changes in the Walker Circulation in Response to Global Warming. *Journal of Climate*, *26*(12), 4038–4048. Retrieved from https://journals.ametsoc.org/view/journals/clim/26/12/jcli-d-12-00531.1.xml doi: 10.1175/JCLI-D-12-00531.1

Durack, P. J., Wijffels, S. E., & Matear, R. J. (2012). Ocean salinities reveal strong global water cycle intensification during 1950 to 2000. *Science*, *336*(6080), 455–458. Retrieved from https://www.science.org/doi/10.1126/science.1212222 doi: 10.1126/SCIENCE.1212222/SUPPL{_}FILE/DURACK.SM.PDF

England, M. H., Mcgregor, S., Spence, P., Meehl, G. A., Timmermann, A., Cai, W., … Santoso, A. (2014). Recent intensification of wind-driven circulation in the Pacific and the ongoing warming hiatus. *Nature Climate Change*, *4*(3), 222–227. doi: 10.1038/nclimate2106

Falster, G., Konecky, B., Madhavan, M., Stevenson, S., & Coats, S. (2021). Imprint of the Pacific Walker Circulation in Global Precipitation δ18O. *Journal of Climate*, *34*(21), 8579–8597. Retrieved from https://journals.ametsoc.org/view/journals/clim/34/21/JCLI-D-21-0190.1.xml doi: 10.1175/JCLI-D-21-0190.1

Gill, A. E. (1980). Some simple solutions for heat-induced tropical circulation. *Quarterly Journal of the Royal Meteorological Society*, *106*(449), 447–462. doi: 10.1002/qj.49710644905

Gulev, S. K., Thorne, P. W., Ahn, J., Dentener, F. J., Domingues, C. M., Gerland, S., ... Vose, R. S. (2021). Changing State of the Climate System. In V. Masson-Delmotte et al. (Eds.), *Climate change 2021: The physical science basis. contribution of working group i to the sixth assessment report of the intergovernmental panel on climate change* (chap. 2). Cambridge, United Kingdom and New York, NY, USA: Cambridge University Press. Retrieved from https://www.ipcc.ch/report/ar6/wg1/downloads/report/IPCC_AR6_WGI_Chapter_02.pdf

He, J., Soden, B. J., & Kirtman, B. (2014). The robustness of the atmospheric circulation and precipitation response to future anthropogenic surface warming. *Geophysical Research Letters*, *41*(7), 2614–2622. Retrieved from https://onlinelibrary.wiley.com/doi/full/10.1002/2014GL059435https://onlinelibrary.wiley.com/doi/abs/10.1002/2014GL059435https://agupubs.onlinelibrary.wiley.com/doi/10.1002/2014GL059435 doi: 10.1002/2014GL059435

Held, I. M., & Soden, B. J. (2006). Robust responses of the hydrological cycle to global warming. *Journal of Climate*, *19*(21), 5686–5699. Retrieved from http://journals.ametsoc.org/jcli/article-pdf/19/21/5686/3800493/jcli3990_1.pdf doi: 10.1175/JCLI3990.1

Hersbach, H., Bell, B., Berrisford, P., Biavati, G., Horányi, A., Muñoz Sabater, J., ... Thépaut, J.-N. (2018a). *ERA5 hourly data on pressure levels from 1959 to present.* Copernicus Climate Change Service (C3S) Climate Data Store (CDS). Retrieved from https://doi.org/10.24381/cds.bd0915c6 doi: 10.24381/cds.bd0915c6

Hersbach, H., Bell, B., Berrisford, P., Biavati, G., Horányi, A., Muñoz Sabater, J., ... Thépaut, J.-N. (2018b). *ERA5 hourly data on single levels from 1959 to present.* Copernicus Climate Change Service (C3S) Climate Data Store (CDS). Retrieved from `https://doi.org/10.24381/cds.adbb2d47` doi: 10.24381/cds.adbb2d47

Hersbach, H., Bell, B., Berrisford, P., Hirahara, S., Horányi, A., Muñoz-Sabater, J., ... Thépaut, J. N. (2020). The ERA5 Global Reanalysis. *Quarterly Journal of the Royal Meteorological Society*, *146*(730), 1999–2049. Retrieved from `https://rmets.onlinelibrary.wiley.com/doi/full/10.1002/qj.3803` doi: 10.1002/qj.3803

Hussain, M. M., & Mahmud, I. (2019). pyMannKendall: a python package for non parametric Mann Kendall family of trend tests. *Journal of Open Source Software*. Retrieved from `https://doi.org/10.21105/joss.01556` doi: 10.21105/joss.01556

Knutson, T. R., & Manabe, S. (1995). Time-mean response over the tropical Pacific to increased CO2 in a coupled ocean-atmosphere model. *Journal of Climate*, *8*(9), 2181–2199. Retrieved from `https://journals.ametsoc.org/view/journals/clim/8/9/1520-0442_1995_008_2181_tmrott_2_0_co_2.xml` doi: 10.1175/1520-0442(1995)008⟨2181:TMROTT⟩2.0.CO;2

Kociuba, G., & Power, S. B. (2015). Inability of CMIP5 Models to Simulate Recent Strengthening of the Walker Circulation: Implications for Projections. *Journal of Climate*, *28*(1), 20–35. Retrieved from `https://journals.ametsoc.org/view/journals/clim/28/1/jcli-d-13-00752.1.xml` doi: 10.1175/JCLI-D-13-00752.1

Kosaka, Y., & Xie, S. P. (2013). Recent global-warming hiatus tied to equatorial Pacific surface cooling. *Nature*, *501*(7467), 403–407. Retrieved from `http://dx.doi.org/10.1038/nature12534` doi: 10.1038/nature12534

Kosovelj, K., Zaplotnik, Z., & Zagar, N. (2022). *Indices of Pacific Walker Circulation strength: trends, correlations and uncertainty (submitted version).* doi: https://doi.org/10.5281/zenodo.7359879

L'Heureux, M. L., Lee, S., & Lyon, B. (2013, 3). Recent multidecadal strengthening of the Walker circulation across the tropical Pacific. *Nature Climate Change 2013 3:6*, *3*(6), 571–576. Retrieved from `https://www.nature.com/articles/`

nclimate1840 doi: 10.1038/nclimate1840

Liu, Z., Jian, Z., Poulsen, C. J., & Zhao, L. (2019, 2). Isotopic evidence for twentieth-century weakening of the Pacific Walker circulation. *Earth and Planetary Science Letters*, *507*, 85–93. doi: 10.1016/J.EPSL.2018.12.002

Luo, J. J., Sasaki, W., & Masumoto, Y. (2012, 11). Indian Ocean warming modulates Pacific climate change. *Proceedings of the National Academy of Sciences of the United States of America*, *109*(46), 18701–18706. Retrieved from https://www.pnas.org/doi/abs/10.1073/pnas.1210239109 doi: 10.1073/PNAS.1210239109/SUPPL{_}FILE/PNAS.201210239SI.PDF

Mann, M. E., Steinman, B. A., Brouillette, D. J., & Miller, S. K. (2021, 3). Multidecadal climate oscillations during the past millennium driven by volcanic forcing. *Science*, *371*(6533), 1014–1019. Retrieved from https://science.sciencemag.org/content/371/6533/1014https://science.sciencemag.org/content/371/6533/1014.abstract doi: 10.1126/SCIENCE.ABC5810

Masson-Delmotte, V., et al. (Eds.). (2021). *IPCC, 2021: Climate Change 2021: The Physical Science Basis. Contribution of Working Group I to the Sixth Assessment Report of the Intergovernmental Panel on Climate Change.*

McGregor, S., Timmermann, A., Stuecker, M. F., England, M. H., Merrifield, M., Jin, F. F., & Chikamoto, Y. (2014). Recent walker circulation strengthening and pacific cooling amplified by atlantic warming. *Nature Climate Change*, *4*(10), 888–892. doi: 10.1038/nclimate2330

Meehl, G. A., Arblaster, J. M., Fasullo, J. T., Hu, A., & Trenberth, K. E. (2011, 9). Model-based evidence of deep-ocean heat uptake during surface-temperature hiatus periods. *Nature Climate Change 2011 1:7*, *1*(7), 360–364. Retrieved from https://www.nature.com/articles/nclimate1229 doi: 10.1038/nclimate1229

Meng, Q., Latif, M., Park, W., Keenlyside, N. S., Semenov, V. A., & Martin, T. (2012). Twentieth century Walker Circulation change: Data analysis and model experiments. *Climate Dynamics*, *38*(9-10), 1757–1773. Retrieved from https://link.springer.com/article/10.1007/s00382-011-1047-8 doi: 10.1007/S00382-011-1047-8/FIGURES/13

Merrifield, M. A. (2011, 8). A Shift in Western Tropical Pacific Sea Level

Trends during the 1990s. *Journal of Climate*, *24*(15), 4126–4138. Retrieved from https://journals.ametsoc.org/view/journals/clim/24/15/2011jcli3932.1.xml doi: 10.1175/2011JCLI3932.1

Muis, S., Haigh, I. D., Guimarães Nobre, G., Aerts, J. C., & Ward, P. J. (2018, 9). Influence of El Niño-Southern Oscillation on Global Coastal Flooding. *Earth's Future*, *6*(9), 1311–1322. Retrieved from https://onlinelibrary.wiley.com/doi/full/10.1029/2018EF000909https://onlinelibrary.wiley.com/doi/abs/10.1029/2018EF000909https://agupubs.onlinelibrary.wiley.com/doi/10.1029/2018EF000909 doi: 10.1029/2018EF000909

Orihuela-Pinto, B., England, M. H., & Taschetto, A. S. (2022, 6). Interbasin and interhemispheric impacts of a collapsed Atlantic Overturning Circulation. *Nature Climate Change 2022 12:6*, *12*(6), 558–565. Retrieved from https://www.nature.com/articles/s41558-022-01380-y doi: 10.1038/s41558-022-01380-y

Peixoto, J. P., & Oort, A. H. (1992). *Physics of climate.* American Institute of Physics.

Pikovnik, M., Zaplotnik, Z., Boljka, L., & Žagar, N. (2022, 6). Metrics of the Hadley circulation strength and associated circulation trends. *Weather and Climate Dynamics*, *3*(2), 625–644. doi: 10.5194/WCD-3-625-2022

Plesca, E., Grützun, V., & Buehler, S. A. (2018, 1). How Robust Is the Weakening of the Pacific Walker Circulation in CMIP5 Idealized Transient Climate Simulations? *Journal of Climate*, *31*(1), 81–97. Retrieved from https://journals.ametsoc.org/view/journals/clim/31/1/jcli-d-17-0151.1.xml doi: 10.1175/JCLI-D-17-0151.1

Power, S. B., & Kociuba, G. (2011). What Caused the Observed Twentieth-Century Weakening of the Walker Circulation? *Journal of Climate*, *24*(24), 6501–6514. Retrieved from https://journals.ametsoc.org/view/journals/clim/24/24/2011jcli4101.1.xml doi: 10.1175/2011JCLI4101.1

Rayner, N. A., Parker, D. E., Horton, E. B., Folland, C. K., Alexander, L. V., Rowell, D. P., … Kaplan, A. (2003, 7). Global analyses of sea surface temperature, sea ice, and night marine air temperature since the late nineteenth century. *Journal of Geophysical Research: Atmospheres*, *108*(D14), 4407. Retrieved from https://onlinelibrary.wiley.com/doi/full/10.1029/

2002JD002670https://onlinelibrary.wiley.com/doi/abs/10.1029/2002JD002670https://agupubs.onlinelibrary.wiley.com/doi/10.1029/2002JD002670 doi: 10.1029/2002JD002670

Sandeep, S., Stordal, F., Sardeshmukh, P. D., & Compo, G. P. (2014, 4). Pacific Walker Circulation variability in coupled and uncoupled climate models. *Climate Dynamics*, *43*(1-2), 103–117. Retrieved from https://link.springer.com/article/10.1007/s00382-014-2135-3 doi: 10.1007/S00382-014-2135-3/FIGURES/9

Seager, R., Cane, M., Henderson, N., Lee, D. E., Abernathey, R., & Zhang, H. (2019, 7). *Strengthening tropical Pacific zonal sea surface temperature gradient consistent with rising greenhouse gases* (Vol. 9) (No. 7). Nature Publishing Group. Retrieved from https://doi.org/10.1038/s41558-019-0505-x doi: 10.1038/s41558-019-0505-x

Simmons, A. J. (2022, 7). Trends in the tropospheric general circulation from 1979 to 2022. *Weather and Climate Dynamics*, *3*(3), 777–809. doi: 10.5194/WCD-3-777-2022

Sohn, B. J., & Park, S.-C. (2010, 8). Strengthened tropical circulations in past three decades inferred from water vapor transport. *Journal of Geophysical Research*, *115*(D15), D15112. Retrieved from http://doi.wiley.com/10.1029/2009JD013713 doi: 10.1029/2009JD013713

Sohn, B. J., Yeh, S. W., Lee, A., & Lau, W. K. (2019, 3). Regulation of atmospheric circulation controlling the tropical Pacific precipitation change in response to CO2 increases. *Nature Communications*, *10*(1), 1–8. Retrieved from https://www.nature.com/articles/s41467-019-08913-8 doi: 10.1038/s41467-019-08913-8

Sohn, B. J., Yeh, S. W., Schmetz, J., & Song, H. J. (2013, 4). Observational evidences of Walker circulation change over the last 30 years contrasting with GCM results. *Climate Dynamics*, *40*(7-8), 1721–1732. Retrieved from https://link.springer.com/article/10.1007/s00382-012-1484-z doi: 10.1007/S00382-012-1484-Z/FIGURES/5

Tanaka, H. L., Ishizaki, N., & Kitoh, A. (2004, 5). Trend and interannual variability of Walker, monsoon and Hadley circulations defined by velocity potential in the upper troposphere. *Tellus A*, *56*(3), 250–269. Retrieved from http://tellusa.net/index.php/tellusa/article/view/14410 doi: 10.1111/j.1600-0870.2004.00049.x

Tokinaga, H., & Xie, S. P. (2011, 1). Wave- and Anemometer-Based Sea Surface Wind (WASWind) for Climate Change Analysis. *Journal of Climate*, *24*(1), 267–285. Retrieved from https://journals.ametsoc.org/view/journals/clim/24/1/2010jcli3789.1.xml doi: 10.1175/2010JCLI3789.1

Tokinaga, H., Xie, S. P., Deser, C., Kosaka, Y., & Okumura, Y. M. (2012, 11). Slowdown of the Walker circulation driven by tropical Indo-Pacific warming. *Nature 2012 491:7424*, *491*(7424), 439–443. Retrieved from https://www.nature.com/articles/nature11576 doi: 10.1038/nature11576

Troup, A. J. (1965, 10). The 'southern oscillation'. *Quarterly Journal of the Royal Meteorological Society*, *91*(390), 490–506. Retrieved from https://onlinelibrary.wiley.com/doi/full/10.1002/qj.49709139009https://onlinelibrary.wiley.com/doi/abs/10.1002/qj.49709139009https://rmets.onlinelibrary.wiley.com/doi/10.1002/qj.49709139009 doi: 10.1002/QJ.49709139009

Vecchi, G. A., & Soden, B. J. (2007, 9). Global Warming and the Weakening of the Tropical Circulation. *Journal of Climate*, *20*(17), 4316–4340. Retrieved from http://journals.ametsoc.org/doi/10.1175/JCLI4258.1 doi: 10.1175/JCLI4258.1

Vecchi, G. A., Soden, B. J., Wittenberg, A. T., Held, I. M., Leetmaa, A., & Harrison, M. J. (2006, 5). Weakening of tropical Pacific atmospheric circulation due to anthropogenic forcing. *Nature 2006 441:7089*, *441*(7089), 73–76. Retrieved from https://www.nature.com/articles/nature04744 doi: 10.1038/nature04744

Wang, C. (2002, 2). Atmospheric circulation cells associated with the El Nino-Southern Oscillation. *Journal of Climate*, *15*(4), 399–419. Retrieved from https://journals.ametsoc.org/view/journals/clim/15/4/1520-0442_2002_015_0399_accawt_2.0.co_2.xml doi: 10.1175/1520-0442(2002)015⟨0399:ACCAWT⟩2.0.CO;2

Watanabe, M., Dufresne, J. L., Kosaka, Y., Mauritsen, T., & Tatebe, H. (2020). Enhanced warming constrained by past trends in equatorial Pacific sea surface temperature gradient. *Nature Climate Change*, *11*, 33–37. doi:

10.1038/s41558-020-00933-3

Watanabe, M., Kamae, Y., Yoshimori, M., Oka, A., Sato, M., Ishii, M., ... Kimoto, M. (2013, 6). Strengthening of ocean heat uptake efficiency associated with the recent climate hiatus. *Geophysical Research Letters*, *40*(12), 3175–3179. Retrieved from https://agupubs.onlinelibrary.wiley.com/doi/full/10.1002/grl.50541https://agupubs.onlinelibrary.wiley.com/doi/abs/10.1002/grl.50541https://agupubs.onlinelibrary.wiley.com/doi/10.1002/grl.50541 doi: 10.1002/grl.50541

Wills, R. C. J., Dong, Y., Proistosecu, C., Armour, K. C., & Battisti, D. S. (2022, 9). Systematic Climate Model Biases in the Large-Scale Patterns of Recent Sea-Surface Temperature and Sea-Level Pressure Change. *Geophysical Research Letters*, *49*(17), e2022GL100011. Retrieved from https://onlinelibrary.wiley.com/doi/full/10.1029/2022GL100011https://onlinelibrary.wiley.com/doi/abs/10.1029/2022GL100011https://agupubs.onlinelibrary.wiley.com/doi/10.1029/2022GL100011 doi: 10.1029/2022GL100011

Woodruff, S. D., Worley, S. J., Lubker, S. J., Ji, Z., Eric Freeman, J., Berry, D. I., ... Wilkinson, C. (2011, 6). ICOADS Release 2.5: extensions and enhancements to the surface marine meteorological archive. *International Journal of Climatology*, *31*(7), 951–967. Retrieved from https://onlinelibrary.wiley.com/doi/full/10.1002/joc.2103https://onlinelibrary.wiley.com/doi/abs/10.1002/joc.2103https://rmets.onlinelibrary.wiley.com/doi/10.1002/joc.2103 doi: 10.1002/JOC.2103

Wu, M., Zhou, T., Li, C., Li, H., Chen, X., Wu, B., ... Zhang, L. (2021, 11). A very likely weakening of Pacific Walker Circulation in constrained near-future projections. *Nature Communications 2021 12:1*, *12*(1), 1–8. Retrieved from https://www.nature.com/articles/s41467-021-26693-y doi: 10.1038/s41467-021-26693-y

Yu, B., & Zwiers, F. W. (2010, 3). Changes in equatorial atmospheric zonal circulations in recent decades. *Geophysical Research Letters*, *37*(5), 5701. Retrieved from https://onlinelibrary.wiley.com/doi/full/10.1029/2009GL042071https://onlinelibrary.wiley.com/doi/abs/10.1029/2009GL042071https://agupubs.onlinelibrary.wiley.com/doi/10.1029/

2009GL042071 doi: 10.1029/2009GL042071

Yue, S., & Wang, C. (2002, 6). Applicability of Prewhitening to Eliminate the Influence of Serial Correlation on the Mann-Kendall Test. *Water Resources Research - WATER RESOUR RES*, *38*(6), 1–4. Retrieved from https://agupubs.onlinelibrary.wiley.com/doi/full/10.1029/2001WR000861 doi: 10.1029/2001WR000861

Zaplotnik, Z., Pikovnik, M., & Boljka, L. (2022, 3). Recent Hadley circulation strengthening: a trend or multidecadal variability? *Journal of Climate*, *-1*(aop), 1–65. Retrieved from https://journals.ametsoc.org/view/journals/clim/aop/JCLI-D-21-0204.1/JCLI-D-21-0204.1.xml doi: 10.1175/JCLI-D-21-0204.1

Zhang, L., & Karnauskas, K. B. (2017, 1). The Role of Tropical Interbasin SST Gradients in Forcing Walker Circulation Trends. *Journal of Climate*, *30*(2), 499–508. Retrieved from https://journals.ametsoc.org/view/journals/clim/30/2/jcli-d-16-0349.1.xml doi: 10.1175/JCLI-D-16-0349.1

Zhao, X., & Allen, R. J. (2019, 4). Strengthening of the Walker Circulation in recent decades and the role of natural sea surface temperature variability. *Environmental Research Communications*, *1*(2), 021003. Retrieved from https://iopscience.iop.org/article/10.1088/2515-7620/ab0dabhttps://iopscience.iop.org/article/10.1088/2515-7620/ab0dab/meta doi: 10.1088/2515-7620/AB0DAB

Indices of Pacific Walker Circulation strength: trends, correlations and uncertainty

Katarina Kosovelj, Žiga Zaplotnik, Nedjeljka Žagar

December 8, 2022

References

A. J. Clarke and A. Lebedev. Long-Term Changes in the Equatorial Pacific Trade Winds. *Journal of Climate*, 9(5):1020–1029, 1996.

D. G. Wright and K. R. Thompson. Time-Averaged Forms of the Nonlinear Stress Law. *Journal of Physical Oceanography*, 13(2):341 – 345, 1983. doi: 10.1175/1520-0485(1983)013⟨0341:TAFOTN⟩2.0.CO;2. URL https://journals.ametsoc.org/view/journals/phoc/13/2/1520-0485_1983_013_0341_tafotn_2_0_co_2.xml.

Table 1: Trends of normalized indices of annual-mean Pacific Walker circulation strength for different periods shown in Fig. 3 in the main text. The values in parentheses denote the standard error of the trend estimates. Stars denote statistical significance of the trend at 95% confidence using Mann-Kendall test. SST, V_e, L_τ and U_{ave} indices are multiplied by (-1) for easier comparison with other indices. Units in columns denote linear trend ($\pm$ 1 σ) in units yr^{-1}.

PWC index	1960-2020	1970-2020	1980-2020	1990-2020	2000-2020
$\chi_{\max}$	0.009 ($\pm$ 0.007)	0.013 ($\pm$ 0.010)*	0.041 ($\pm$ 0.012)*	0.050 ($\pm$ 0.019)*	-0.007($\pm$ 0.026)
SOI	0.003 ($\pm$ 0.007)	-0.005 ($\pm$ 0.009)	0.015 ($\pm$ 0.011)	0.023 ($\pm$ 0.017)	-0.003 ($\pm$ 0.031)
ΔSLP	-0.007 ($\pm$ 0.007)	-0.006 ($\pm$ 0.010)	0.014 ($\pm$ 0.013)	0.020 ($\pm$ 0.019)	-0.020 ($\pm$ 0.030)
ω_{500}	-0.003 ($\pm$ 0.008)	0.003 ($\pm$ 0.011)	0.027 ($\pm$ 0.014)*	0.045 ($\pm$ 0.022)*	-0.017 ($\pm$ 0.030)
ψ_{500}	-0.010 ($\pm$ 0.007)	-0.012 ($\pm$ 0.009)	0.007 ($\pm$ 0.012)	0.022 ($\pm$ 0.017)	-0.003 ($\pm$ 0.031)
-SST	0.006 ($\pm$ 0.007)	0.007 ($\pm$ 0.010)	0.019 ($\pm$ 0.014)	0.026 ($\pm$ 0.019)	-0.014 ($\pm$ 0.029)
-V_e	-0.015 ($\pm$ 0.007)	-0.013 ($\pm$ 0.010)	0.001 ($\pm$ 0.013)	0.013 ($\pm$ 0.020)	-0.016 ($\pm$ 0.032)
Q_{200}	-0.001 ($\pm$ 0.007)	-0.001 ($\pm$ 0.011)	0.024 ($\pm$ 0.015)	0.046 ($\pm$ 0.020)*	0.006 ($\pm$ 0.029)
-L_τ	-0.002($\pm$ 0.007)	0.002 ($\pm$ 0.010)	0.026 ($\pm$ 0.013)*	0.047 ($\pm$ 0.020)*	-0.012 ($\pm$ 0.031)
-U_{ave}	-0.007 ($\pm$ 0.007)	-0.005 ($\pm$ 0.010)	0.021 ($\pm$ 0.014)	0.041 ($\pm$ 0.021)*	-0.016 ($\pm$ 0.032)

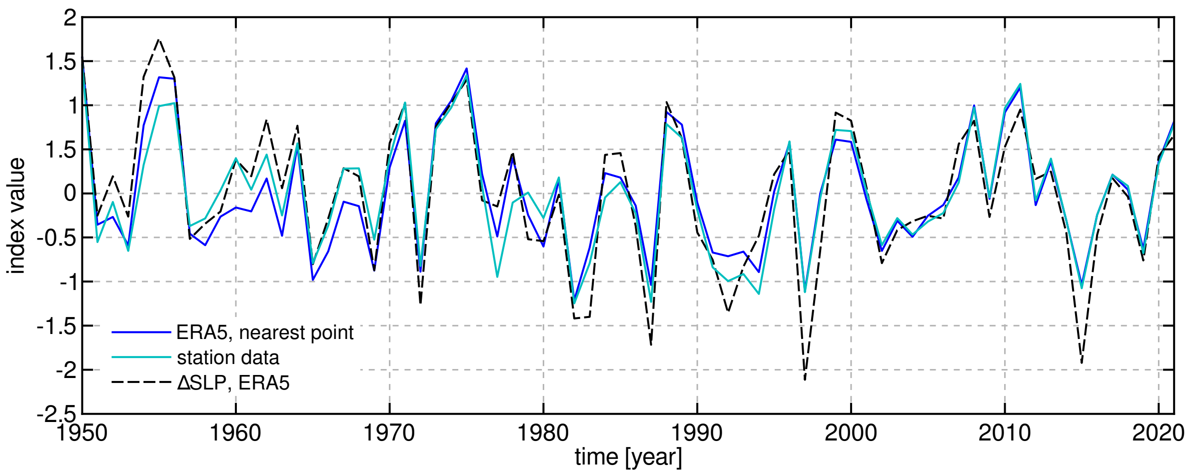

Figure S1: Time series of annual-mean Troup SOI (divided by 10), computed from ERA5 reanalysis using nearest gridpoints to Tahiti and Darwin stations, and NCAR Climate Data Guide station data time series. ΔSLP index computed from ERA5 data is added for comparison. Nearest point method produces almost identical values as bilinear interpolation of surface pressure data to station locations (not shown). The difference decrease significantly in the recent period, most likely due to the steady improvement of reanalysis accuracy when more observations are assimilated.

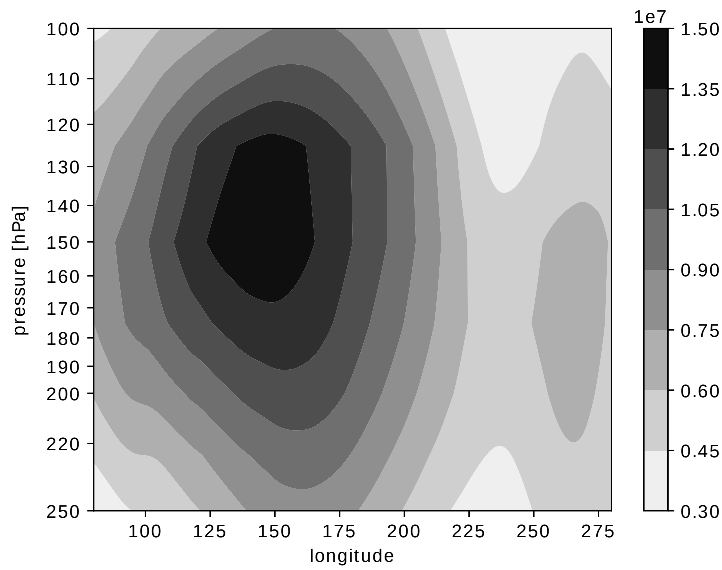

Figure S2: Maximal absolute value of χ (in s^{-1}) between 25°S and 25°N, in the upper troposphere over equatorial Pacific, averaged over 1951-2020.

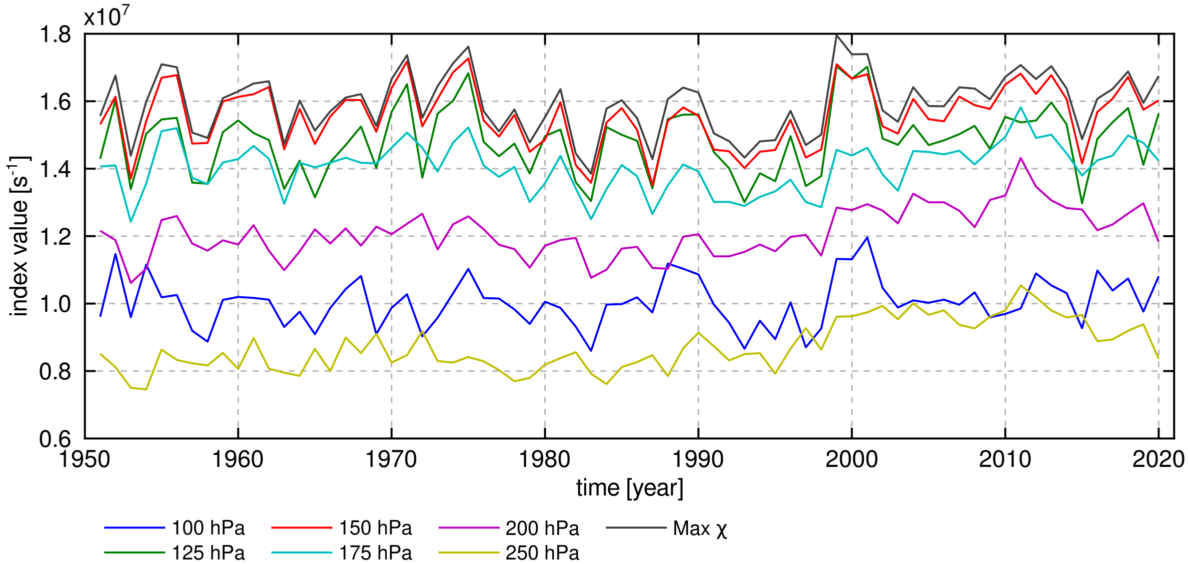

Figure S3: Time series of annual-mean values of χ index at different vertical levels. On average, 150 hPa level is the level closest to maximal divergent outflow in the upper-tropospheric branch of PWC, as χ at 150 hPa is almost perfectly correlated to the data-adaptive index of maximum velocity potential χ_{max} ($r = 0.98$). The latter is computed as a maximum of monthly-mean velocity potential (divergent outflow) at any pressure level in the troposphere.

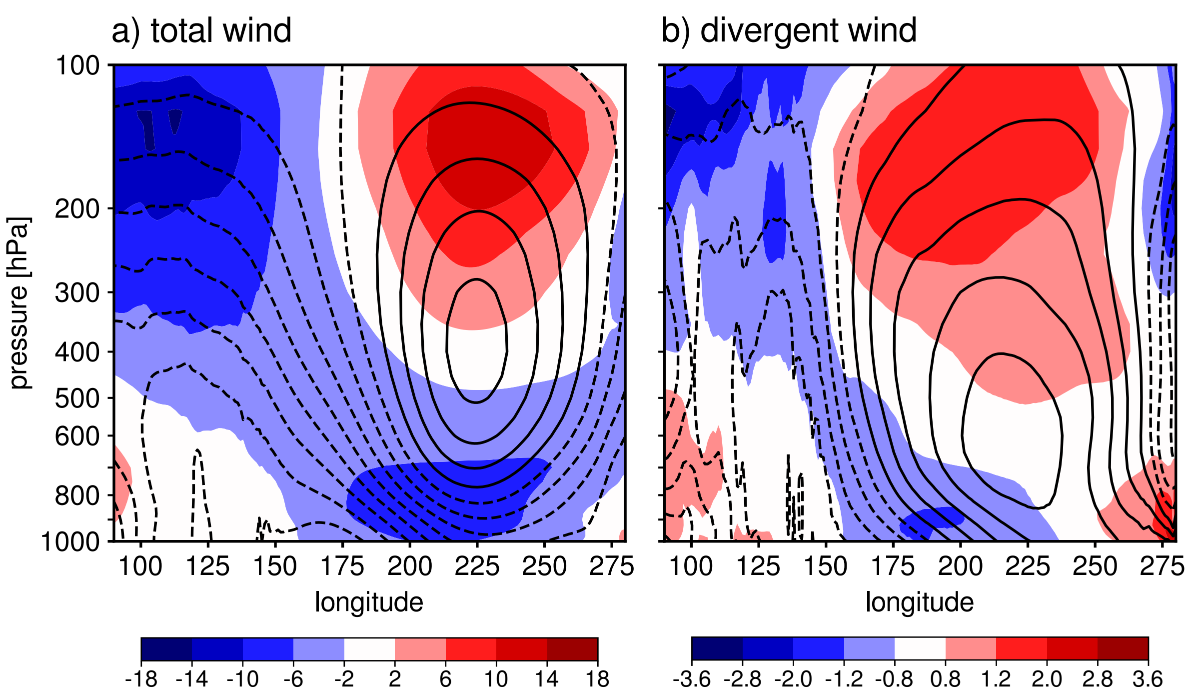

Figure S4: Vertical cross section of zonal wind (colors, in m/s) and mass stream function (contours), averaged over period 1950-2021 and from 5°S to 5°N. a) for total wind (contours every 2×10^{11} kg/s) and b) for divergent wind (contours every 0.4×10^{11} kg/s)

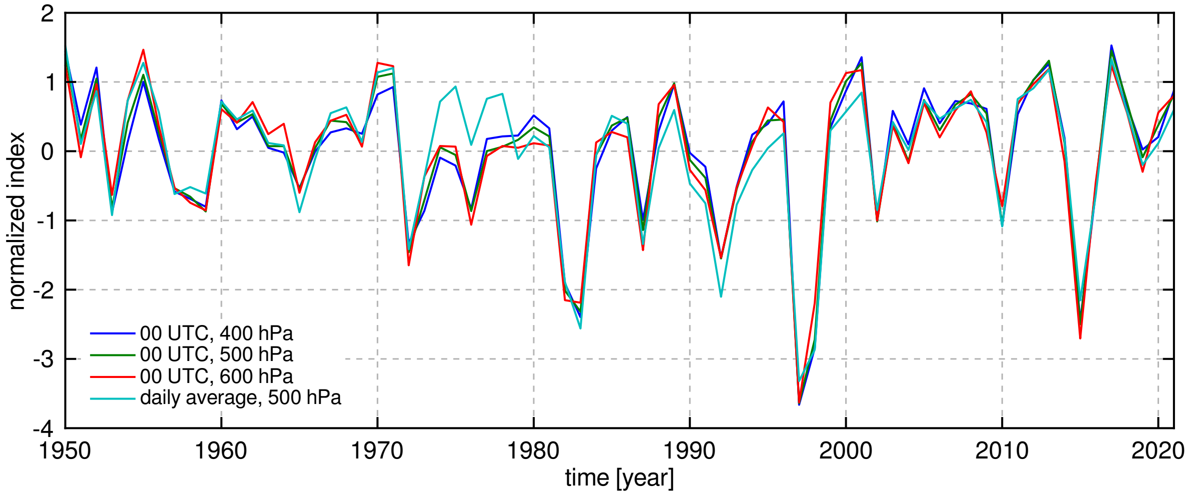

Figure S5: Time series of ω-indices of Pacific Walker circulation strength in ERA5 reanalysis between 1950 and 2021. Different ω-indices, computed from hourly data at 00 UTC or daily mean data at different pressure levels (400, 500, 600 hPa) are compared. Time series are normalized by their standard deviation. The indices are largely insensitive to the vertical level or to the data used (daily-mean data or 00 UTC) with their correlations higher than 0.95 for any pair of presented indices.

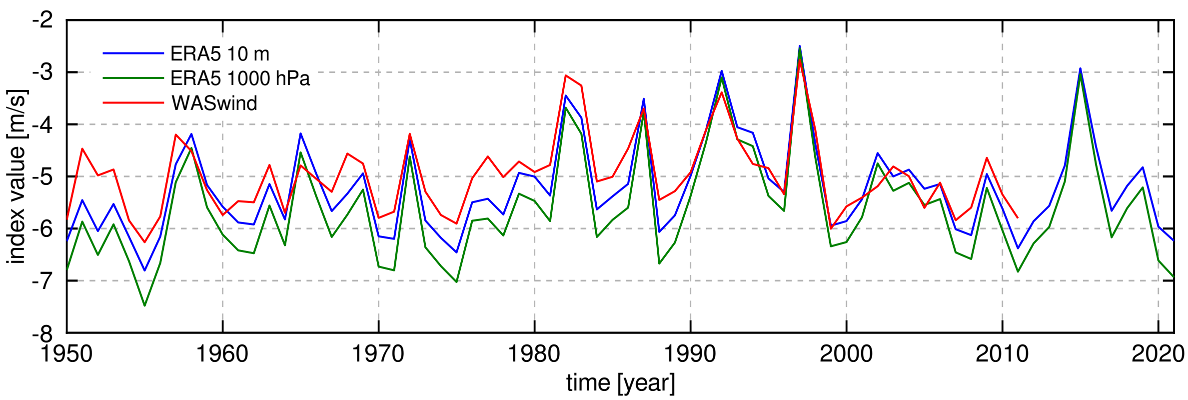

Figure S6: Time series of annual-mean U_{ave} index from ERA5 (at 10 m and at 1000 hPa) and from raw WASwind data.

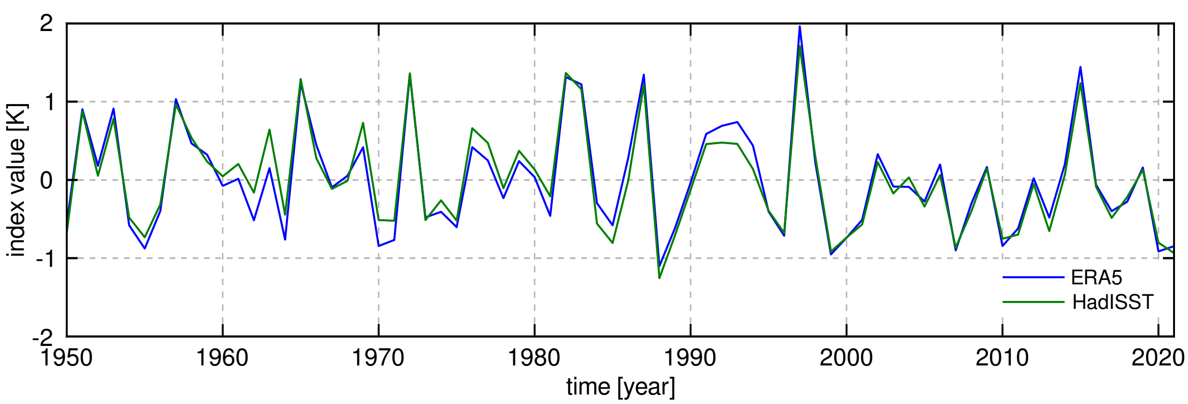

Figure S7: Time series of annual-mean SST index from ERA5 and from raw HadISST data.

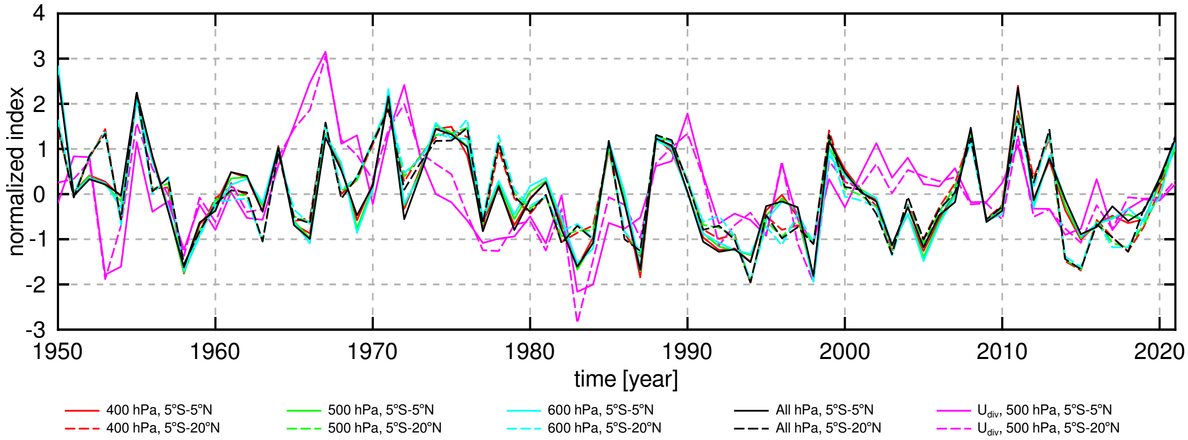

Figure S8: Time series of different variations of normalized ψ index from total zonal wind (annual means), at different vertical levels and for different meridional extent of areas over which wind was averaged. Vertical pressure level stands for indices computed as maximal mass stream function at particular level, "All hPa" denotes index, computed as maximal stream function in the zonal-vertical cross section, and "U_{div}" denotes index, computed from divergent component of zonal wind.

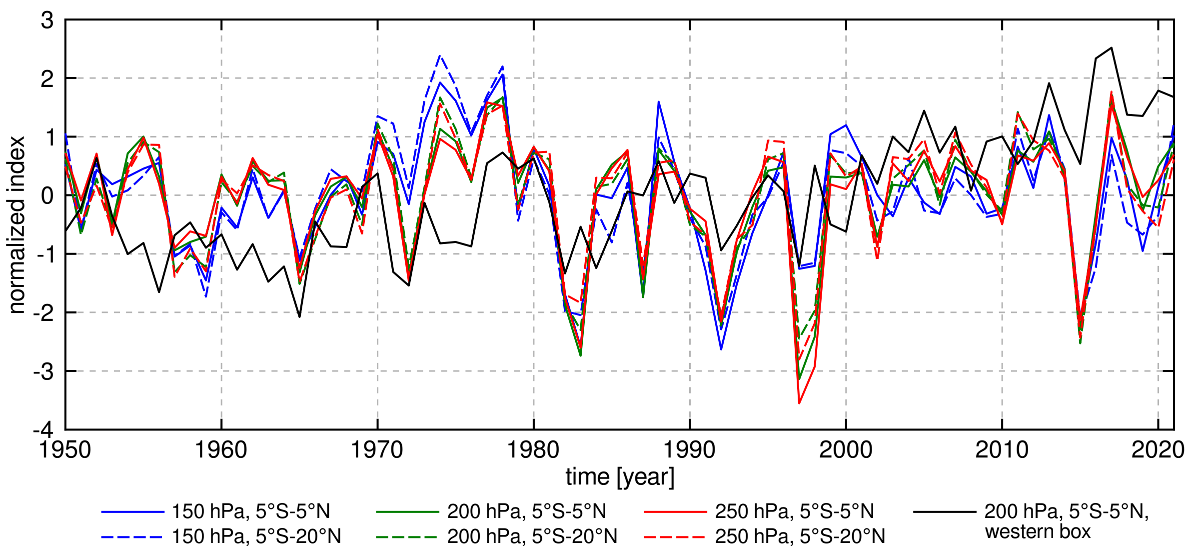

Figure S9: Time series of normalized annual mean values of Q index, calculated at different pressure levels, averaged over areas with different meridional extent. The index is largely insensitive to the change of meridional extent ($r > 0.94$ for any pair of indices). The same applies in the case of change in vertical level from 200 to 250 hPa ($r > 0.98$), whereas differences are larger in the case of change to 150 hPa ($r = 0.8$). Black line represent Q index computed from the western Pacific box only, without subtraction of values from the eastern Pacific box. The index does not distinguish circulation signal from the climate-change induced thermodynamic signal.

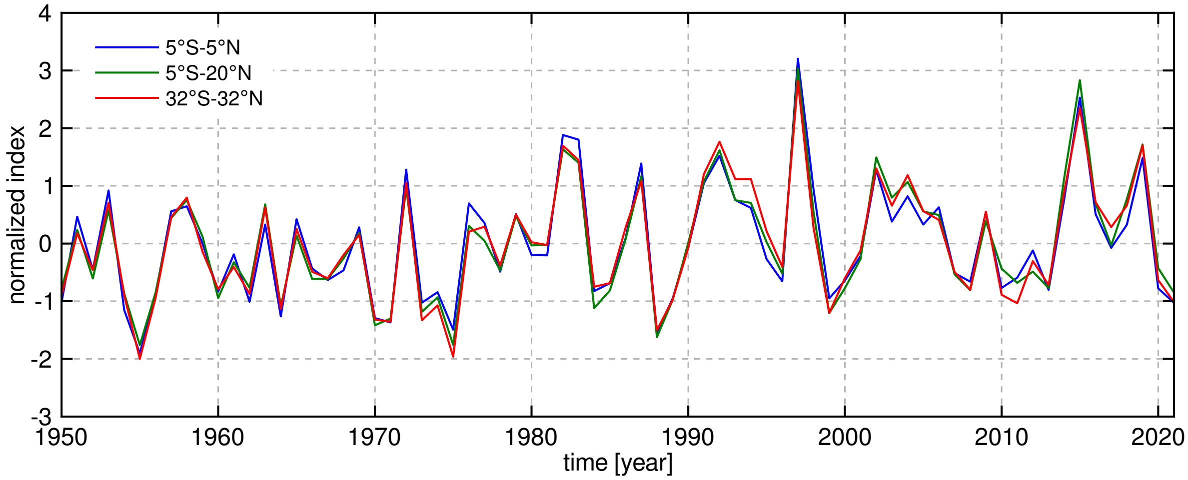

Figure S10: Time series of normalized annual means of V_e index computed for different meridional extent of horizontal areas: narrow tropical belt (5°S to 5°N) as in the main text; belt around ITCZ (5°S to 20°N), whole tropical belt (32°S to 32°N). Normalized V_e index show little sensitivity to change in meridional extent of area for computation of the index ($r > 0.97$).

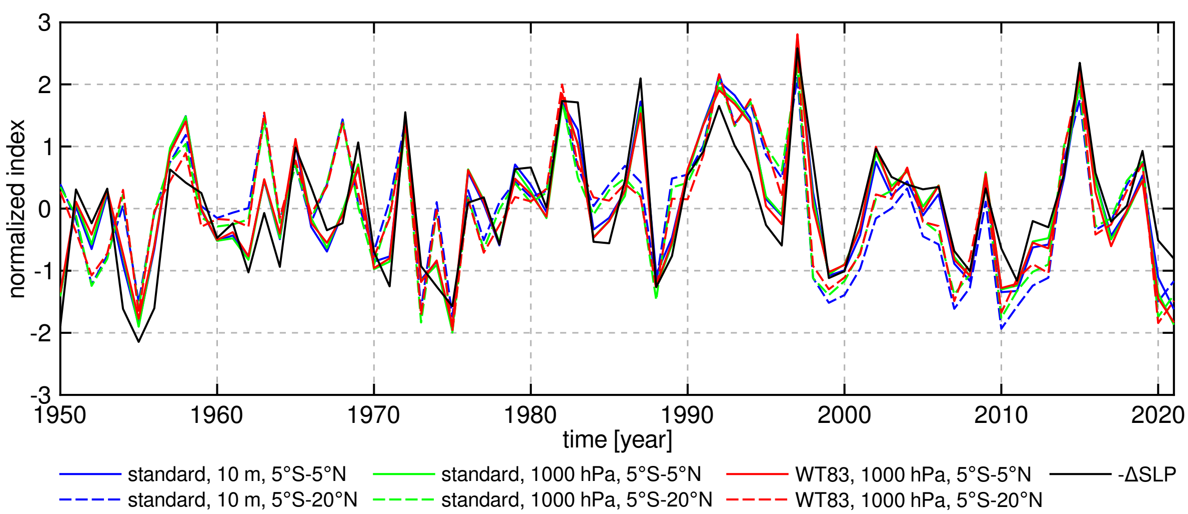

Figure S11: Time series of normalized annual mean values of L_τ index, computed from "standard" formula (Clarke and Lebedev, 1996) at 10 m and 1000 hPa, and following Wright and Thompson (1983) at 1000 hPa. For comparison, ΔSLP index multiplied by (-1) is added to the plot for comparison. Wind stress index is more sensitive to the change in meridional extent of horizontal area used for calculation of index than to the change in calculation of τ_x

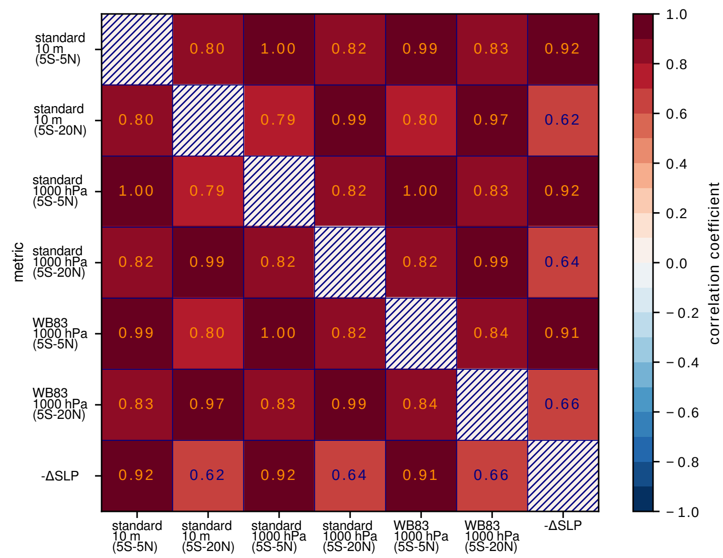

Figure S12: Correlation coefficients between different variations of L_τ index, and between different variations of L_τ index and ΔSLP index. High correlations with ΔSLP confirm the findings of Clarke and Lebedev (1996) that the wind-stress index and surface pressure index may be used interchangeably when studying multidecadal variability.